frontiers | Frontiers in Earth Science

TYPE Original Research
PUBLISHED 03 November 2022
DOI 10.3389/feart.2022.909951

OPEN ACCESS

EDITED BY
Alison Hollomon Graettinger,
University of Missouri–Kansas City,
United States

REVIEWED BY
Felipe Aguilera,
Catholic University of the North, Chile
Matthew Sweeney,
Los Alamos National Laboratory (DOE),
United States

*CORRESPONDENCE
Göksu Uslular,
goeksu.uslular@etu.unige.ch,
goksu.uslular@tubitak.gov.tr

SPECIALTY SECTION
This article was submitted to Volcanology,
a section of the journal
Frontiers in Earth Science

RECEIVED 31 March 2022
ACCEPTED 07 October 2022
PUBLISHED 03 November 2022

CITATION
Uslular G, Gençalioğlu Kuşcu G, Bégué F, Ruch J, Lupi M, Higgins O and Caricchi L (2022), New findings on compositionally distinct maar volcanoes: A case study from Acıgöl (Nevşehir) caldera (Central Anatolia, Turkey).
Front. Earth Sci. 10:909951.
doi: 10.3389/feart.2022.909951

New findings on compositionally distinct maar volcanoes: A case study from Acıgöl (Nevşehir) caldera (Central Anatolia, Turkey)

Göksu Uslular[1,2,3]*, Gonca Gençalioğlu Kuşcu[1], Florence Bégué[2], Joël Ruch[2], Matteo Lupi[2], Oliver Higgins[2] and Luca Caricchi[2]

[1]Department of Geological Engineering, Muğla Sıtkı Koçman University, Kötekli Campus, Muğla, Turkey, [2]Department of Earth Sciences, University of Geneva, Geneva, Switzerland, [3]TÜBİTAK Marmara Research Centre, Polar Research Institute, Gebze/Kocaeli, Turkey

Recent experiments have largely reshaped our knowledge of maar volcanism. A new evolutionary model promoting the role of explosion depth and vent migration during the formation of maars has provided an alternative approach to previous models. Despite a few attempts to test this model with real cases, there is still a need for field-based studies exploring the depositional characteristics of maars to better understand the factors affecting the model constraints. More investigations on less known felsic maars are required to elucidate the possible differences from their more common mafic counterparts. Here, we explore compositionally distinct monogenetic clusters within the Acıgöl caldera (NW of Central Anatolian Volcanic Province, CAVP), with four felsic maars (İnallı, Kalecitepe, Acıgöl, and Korudağ) and one mafic maar (İcik). Our field observations reveal a successive formation between rhyolitic maars and adjacent lava domes. The mugearitic İcik coalescent maar and the adjacent scoria cone are synchronously formed, which is disclosed by the intercalation of the maar and scoria cone deposits. The geochemistry of the maar juveniles suggests a parental basaltic magma source that has been possibly differentiated by varying degrees of fractional crystallization. Our findings identify the main factors in maar formation (i.e., optimum scaled depth-OSD, water-magma interaction, and basement lithology). We also determine some differences between the felsic and mafic maars in the region, such as higher juvenile content, less amount of sedimentary structure, and a clear transition from phreatomagmatic to magmatic explosions through the end of stratigraphy. All these reflect the complexity of maars, mainly formed by different depths of explosions that occurred in the shallowest few hundred meters rather than a systematic incremental decrease of the eruption locus. Further geophysical and geochronological studies will complete our proposed evolutionary model for the youngest monogenetic activity in the Acıgöl caldera that would also warrant volcanic hazard assessment due to the presence of low-velocity anomalies, shallow Curie depths, and prevalent geothermal activity.

KEYWORDS

crust–magma interaction, maar, bimodal magmatism, monogenetic volcanism, Central Anatolia

Introduction

Monogenetic volcanoes, irrespective of their etymological meaning, have complex evolutionary mechanisms which generally include more than one eruption style in their short eruptive history (Carrasco-Núñez and Riggs, 2008; Martí et al., 2011; van Otterloo et al., 2013; Chako-Tchamabé et al., 2016). Investigating the exposed deposits of monogenetic volcanoes is a key method to fingerprint the changes in eruption dynamics during their formation (Valentine et al., 2005; Riggs and Duffield, 2008; Di Traglia et al., 2009; Hintz and Valentine, 2012; Ersoy et al., 2019). In addition to the variation of physical parameters (e.g., density and grain size), evidence of stratigraphic geochemical variations has also been reported (Jankovics et al., 2015; Higgins et al., 2021). These volcanoes commonly form complex monogenetic volcanic fields and mostly result from the lateral migration of the dike-fed magma system (Cañón-Tapia, 2016; Kósik et al., 2019; Acocella, 2021).

Maar volcanoes (hereafter maars) are the second most common edifices of monogenetic volcanic fields and serve as a natural laboratory for the investigation of dike propagation and substrata geology (Lorenz, 1973, 1986, 2003; Geshi et al., 2011; White and Ross, 2011; Valentine et al., 2017). Maars are dominantly generated by phreatomagmatic eruptions, including either one major (Sato and Taniguchi, 1997) or, more typically, many discrete explosions (Taddeucci et al., 2010) where the molten fuel–coolant interaction (MFCI) happens between the rising magma and groundwater (i.e., explosion locus; Lorenz, 1986). The eruption style of maars is not limited to phreatomagmatic activity similar to other monogenetic volcanoes (e.g., various types of magmatic eruptions in scoria cones; Valentine et al., 2005; Kereszturi and Németh, 2016) as either magmatic or steam-hosted phreatic eruptions can be evident from their short eruptive history (Houghton and Schmincke, 1986; Carrasco-Núñez et al., 2007; Valentine et al., 2017). The various types of base surges and ballistic curtains, together with rarely observed fallouts, are the main deposits observed in maar ejecta (or tephra) rings (Graettinger and Valentine, 2017). Unlike previous models claiming a progressive deepening of the explosion locus and, relevantly, the crater formation (Lorenz, 1986), recent experiment-based studies of maar eruption dynamics favor a vertical (with respect to the scaled depth (SD), an empirical ratio between depth and energy of the explosion; Goto et al., 2001) and lateral movement of explosions and suggest that pre-existing topography (Sweeney et al., 2018; Acocella, 2021) and substrata lithology are the main factors affecting maar formations (Graettinger et al., 2015; Valentine et al., 2017; Sweeney et al., 2018). These factors have been tested by an increasing number of field observations, mostly on mafic maars (Amin and Valentine, 2017; Chako-Tchamabé et al., 2020; De León-Barragán et al., 2020; Ureta et al., 2021), which are significantly more common as compared to their felsic counterparts (Graettinger, 2018). There is still less information on felsic maars due to the limited exposure (Borrero et al., 2017), and hence, their characteristics have been mostly adopted by tuff rings (Ross et al., 2017).

In order to increase the field evidence of recent evolutionary models (Valentine et al., 2017) and enhance the available knowledge on felsic maars, here, we provide a detailed investigation of four felsic maars (İnallı, Kalecitepe, Acıgöl, and Korudağ) and one mafic maar (İcik) found within the Quaternary Acıgöl (or Kocadağ) caldera, the north-western part of the Central Anatolian Volcanic Province (CAVP; Figures 1A and B and Table 1). The CAVP is represented by widespread ignimbrites (Aydar et al., 2012), and several hundreds of monogenetic volcanoes (predominantly scoria cones and several well-exposed maars; Toprak, 1998; Uslular et al., 2021). Most studies in the CAVP focus on the petrological evolution of the widespread volcanism (since ~13 Ma), which remains heavily debated. The main issue is the lack of a clear transition from orogenic to anorogenic volcanism contrary to most post-collisional settings (Lustrino and Wilson, 2007) and the suggested inheritance of a metasomatic mantle source to explain the geochemical signature of the volcanic products (Gençalioğlu-Kuşcu and Geneli, 2010; Reid et al., 2017; Di Giuseppe et al., 2018; Doğan-Külahçı et al., 2018; Rabayrol et al., 2019; Uslular and Gençalioğlu-Kuşcu, 2019; Gall et al., 2021). Maars have received much less attention, with so far only a few studies aiming at deciphering their physical and geochemical characteristics (Keller, 1974; Gevrek and Kazancı, 2000; Gençalioğlu-Kuşcu et al., 2007; Gençalioğlu-Kuşcu, 2011), despite the presence of various deposits and morphologies and both felsic and mafic maars.

The maars and their adjacent monogenetic volcanoes form two distinct clusters in the Acıgöl caldera (NW-SE and N-S trends), which represent some of the youngest monogenetic activity in the CAVP (Türkecan et al., 2004; Schmitt et al., 2011). Despite some preliminary studies on the maar deposits (Kazancı et al., 1995; Türkecan et al., 2004), there is no detailed study assessing the depositional and petrological characteristics of the maars in the region, similar to the rest of the CAVP. Here, we use an integrated approach based on the physical volcanology (e.g., componentry, bulk density, and juvenile inner morphology) and geochemical characterization (whole rock, glass, and mineral chemistry) of both felsic (except for the Kalecitepe that has no exposure) and mafic maars found within the same volcanic field. Our field- and laboratory-based analyses on the exposed maar deposits reveal that both

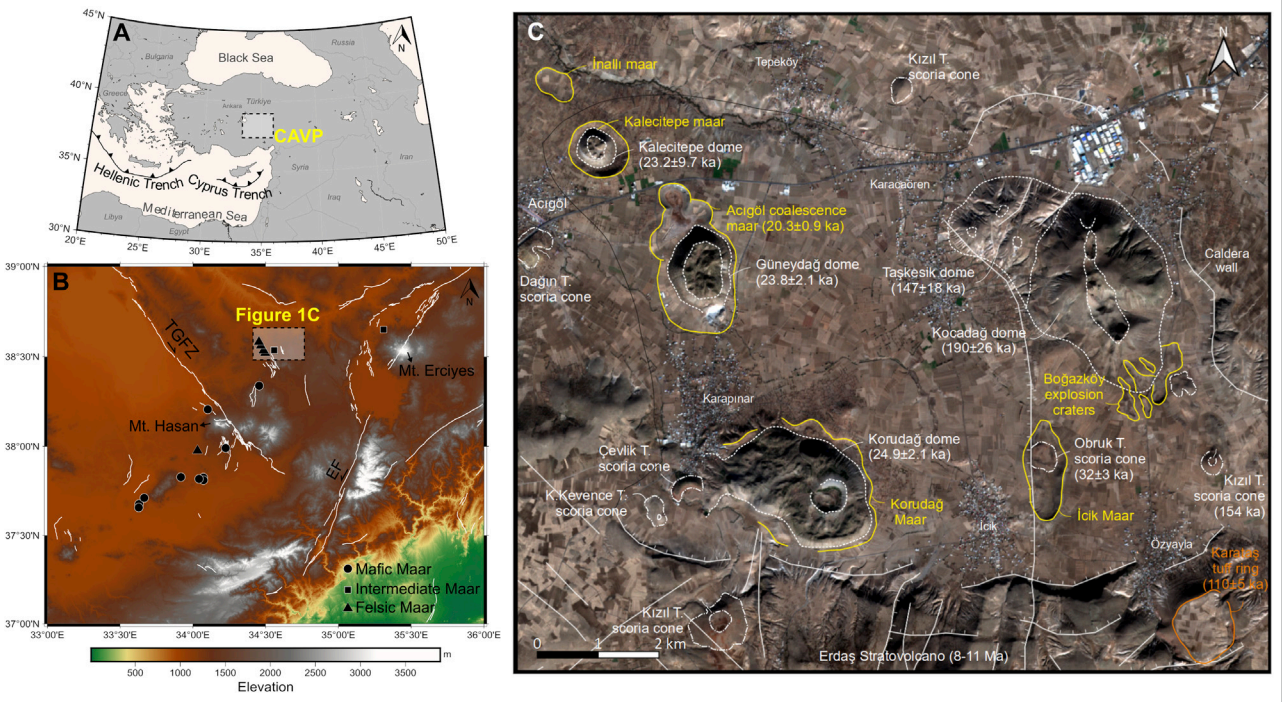

FIGURE 1
(A) Physical map pointing out the locations of active trenches and the CAVP; **(B)** digital elevation model (30 m-resolution SRTM) of the CAVP showing the maars; TGFZ: Tuz Gölü Fault Zone; EF: Ecemiş Fault; **(C)** general view of volcanics in and around the Acıgöl caldera displayed on Sentinel-2 imagery (2019, B4-B3-B2 band combination *via* Semi-Automatic Classification QGIS plugin; Congedo, 2021). The maps in A and B were created using the PyGMT (a Python wrapper for the Generic Mapping Tools; Uieda et al., 2021). Age references are Türkecan et al. (2004), Aydar et al. (2011), and Schmitt et al. (2011). Faults are from Genç and Yürür (2010) and Emre et al. (2011).

vertical and lateral migrations of the explosion locus are evident during the formations of studied maars in line with the recent scaled depth-based evolutionary model. The transition between phreatomagmatic and magmatic explosions (either successive or coeval) identified in both edifice- and outcrop-scale within the studied monogenetic clusters elucidates the dynamic evolutionary mechanisms of maars possibly driven by the changes in scaled depth, magma flux, and hydrogeological properties of the substrata. The compositionally distinct maars are possibly derived from a parental basaltic magma source with different degrees of differentiation. We also highlight the need for further age data obtained directly from maars in the region, as the lava domes in the western cluster should be younger than the adjacent maars, which is contradictory to the available ages (i.e., Acıgöl maar, 20.3 ± 0.9 ka; Güneydağ lava dome, 23.8 ± 2.1 ka; 2σ, U-Th/He, Schmitt et al., 2011; Table 1). Our recent findings, specifically for rarely known felsic maars (e.g., higher juvenile content and less amount of sedimentary structure) and other local outcomes for the Acıgöl region, provide insights into the emplacement of small-volume intrusions beneath complex monogenetic clusters and also the similarities and differences between felsic and mafic maars.

Geological setting

Acıgöl caldera in the northern part of the CAVP hosts ignimbrite deposits (namely, Kumtepe, Aydar et al., 2012) and various post-caldera monogenetic volcanoes (Yıldırım and Özgür, 1981; Druitt et al., 1995; Froger et al., 1998; Mouralis et al., 2002; Ulusoy et al., 2009; Schmitt et al., 2011) (Figure 1C). The Quaternary volcanics in the region overlies the pre-caldera lavas (Yıldırım and Özgür, 1981), ignimbrites (Aydar et al., 2012), and crystalline basement rocks (granitoids, ophiolites, and metamorphics; Floyd et al., 1998). There is no consensus on the exact location and the boundaries of the Acıgöl caldera, but based on the available field and geophysical data, it is likely an ellipsoidal shape of 8 by 12 km (Yıldırım and Özgür, 1981; Ulusoy et al., 2009). This also prevents building a link between the caldera system and post-caldera activity. The Kumtepe ignimbrite consists of two successive eruptive units separated by paleosols and scoria fall deposits, namely, the lower and upper Acıgöl tuffs (LAT and UAT, respectively; Druitt et al., 1995; Aydar et al., 2011). The recently updated ages of these deposits are 190 ± 11 ka (LAT) and 164 ± 4 ka (UAT; 1σ; U-Th/He on zircon; Atıcı et al., 2019). The post-caldera rhyolitic lava domes (Türkecan et al., 2004; Siebel et al.,

TABLE 1 General characteristics of maar volcanoes within the Acıgöl caldera.

Maar	Composition	Age (ka) ± 2σ	Edifice morphology	Ejecta ring and thickness	Juvenile content	Juvenile clast mineralogy	Juvenile clast morphology	Lithic content
İnallı	Rhyolite[a]	n.a.	Individual maar crater	Both proximal (3 m) and mid-distal (1–1.5 m)	Pumice, perlite, and obsidian	Mostly aphyric	Elongated and tube-like pumices	Mostly granitoids with subordinate ophiolites, ignimbrite-derived pinkish pumices, and undifferentiated rocks
Kalecitepe	Rhyolite[b]	≥23.2 ± 9.7 lava dome[c]	Compound craters (maar + lava dome)	No exposure	n.a.	n.a.	n.a.	n.a.
Acıgöl	Rhyolite[a]	20.3 ± 0.9 maar obsidian[c]	Both coalescent (at least 3 maar craters) and compound craters (maar + lava dome)	Only proximal (5–10 m)	Pumice, perlite, and obsidian	Mostly aphyric	Slightly elongated pumices with dense and vesicular types	Mostly granitoids and andesites with subordinate ophiolites, ignimbrite-derived pinkish pumices, and undifferentiated rocks
Korudağ	Rhyolite[a]	≥24.3 ± 2.1 lava dome[c]	Compound craters (a deformed maar crater + lava dome complex)	Only mid-distal (6 m)	Pumice, perlite, and obsidian	Mostly aphyric	Expanded and equant pumices with tube-like vesicles	Granitoids, andesites, and undifferentiated rocks
İcik	Mugearite[a]	≥32 ± 3[d] mid-distal scoria either from scoria cone or maar	Both coalescent (at least 2 maar craters) and compound craters (including a deformed scoria cone)	Proximal (9 m) and mid-distal (15 cm)	Scoria and cauliflower bomb	Olivine and plagioclase microphenocrysts	Equant scoria with coalescent vesicles	Mostly rhyolites and scoria cone-related agglomerates, andesites, obsidians, pumices, and undifferentiated rocks

[a]This study.
[b]Adapted from Kalecitepe lava dome (Siebel et al., 2011).
[c]Schmitt et al. (2011).
[d]Türkecan et al. (2004).

2011) are the most abundant monogenetic edifices in Acıgöl caldera (Figure 1C). They form two spatially and temporally distinct clusters: the first one consists of older lava domes in the eastern part (hereafter, eastern domes; e.g. Kocadağ, 190 ± 26 ka; Taşkesik, 213 ± 18 ka; (U-Th)/He, 2σ, Schmitt et al., 2011) and the second one includes younger lava domes in the western part (hereafter, western domes; e.g. Kalecitepe, 23.2 ± 9.7 ka; Korudağ, 24.3 ± 2.1 ka; 2σ, U-Th/He, Schmitt et al., 2011; Table 1).

Maars, tuff rings, and explosion craters are the second-most common monogenetic volcano type in the region. They are dominantly felsic in composition, except for the mafic İcik maar and Karataş tuff ring (Türkecan et al., 2004; Aydar et al., 2011; and this study). Among the maars, the Acıgöl coalescent maar (20.3 ± 0.9 ka, 2σ, U-Th/He, Schmitt et al., 2011; Table 1) is the only one studied for its volcanological and paleoclimatological characteristics (Kazancı et al., 1995; Roberts et al., 2001; Mouralis et al., 2002, 2019; Tuncer et al., 2019). All felsic maars in the region, except for the İnallı maar (Figure 1C), have a lava dome in their centers that successively postdates the maar formation (Schmitt et al., 2011). Scoria cones of basaltic to andesitic composition are less voluminous (Figure 1C), and their formation is older based on the available geochronological data (32–620 ka, K-Ar; Türkecan et al., 2004; Table 1).

Materials and methods

In line with our main objectives, which are to investigate the depositional and geochemical characteristics of felsic and mafic maars in the Acıgöl caldera and to elucidate their possible evolutionary models and magma sources, we deployed several methods at both field- and juvenile clast-scale, such as fieldwork (e.g., sampling, measuring, and characterizing juvenile and lithic clasts and mapping), sedimentological analysis (sieve analysis and componentry), bulk density measurements, scanning electron microscope acquisition, and geochemical analyses (mineral and whole geochemistry). The first two methods are mostly related to the characterization of exposed maar deposits, whereas the remaining methods aim to explore the physical and geochemical features of maar juvenile clasts to better understand the possible changes in eruption styles during the formation of maars. Details of each method are given in the following sections.

TABLE 2 General overview of maar lithofacies described in both felsic and mafic maars.

Code	Lithofacies	Characteristics	Interpretation
TBm_1	Massive tuff breccia	Massive-bedded, lithic block-bearing (predominantly granites with subordinate ophiolites), ash-rich matrix-supported, medium to coarse lapilli represented by juvenile pumice, obsidian, and perlite, a few sedimentary structures (e.g., impact sags), only observed in felsic maars	Ballistic curtain deposits[a] or high-energy pyroclastic density currents[b] Possible stage of crater widening with the dry phreatomagmatic (or volatile-driven) explosions near or slightly shallower than the optimal scaled depth
TBm_2	Massive tuff breccia	Massive-bedded, block-sized (up to 40 cm) juvenile-rich, ash- to lapilli-rich matrix supported, limited lithic fragments, always located at the top of the stratigraphy, only observed in felsic maars	Ballistic curtain deposits formed by magmatic volatile driven activity with a very limited contribution of phreatomagmatic (i.e., dome/plug explosions; Austin-Erickson et al., 2011)
TBm_3	Massive tuff breccia	Massive to crudely stratified, lapilli to block-sized lithic-rich (65% in İcik maar), limited amounts of juvenile (scoria in İcik maar, and pumice, obsidian and perlite in felsic maars) observed in both felsic and mafic maars, no sedimentary structure	Ballistic curtain deposits[a] or high-energy pyroclastic density currents[b]
AT_1	Ash lapilli tuff	Planar-bedded, well-stratified, alternation with thin ash to lapilli layers, moderately to well-sorted, juvenile-rich in felsic maars and poor in İcik maar	Low-concentration (or dilute) turbulent base surges driven by suspension and traction sedimentation[c]
AT_2	Ash lapilli tuff	Massive to undulatory bedded, well-stratified (especially in Korudağ maar), bearing various low-angle dunes (anti, climbing) in the ash-rich layers, scour channels and impact sags (most common in İcik maar)	Low-concentration base surges with high shear stress[c]
LT	Lapilli tuff	Clast-supported, lapilli-rich, lithic poor	Lapilli fallout deposits possibly formed volatile-driven phreatomagmatically poor explosions
sc	Scoria cone	Agglomerate, bomb, gray-colored ash, only observed in İcik maar	Scoria cone deposits

[a]Graettinger and Valentine (2017).
[b]Branney and Kokelaar (2002).
[c]Sohn and Chough (1989).

Sedimentology and stratigraphy

We studied the depositional characteristics of maars within the Acıgöl caldera from the representative stratigraphic sections of both proximal and mid-distal deposits. Scoria for mafic maar and pumice, perlite, and obsidian for felsic maars refer to the maar juveniles in case they are thought to be derived from the studied maar. We used the terminology for the bedding characteristics (e.g., sedimentary structures and thickness) adopted from Ingram (1954), while we followed White and Houghton (2006) and Blott and Pye (2001) for the grain size and sorting terms, respectively. We described the maar lithofacies following the nomenclatures of Branney and Kokelaar (2002) for ignimbrites and Sohn and Chough (1989) and Graettinger and Valentine (2017) for the ejecta ring deposits (Table 2). All maar deposits are unconsolidated, but the tuff term is just preferred in the described lithofacies to abide by the nomenclature (Table 2). The massive tuff breccia (TBm) with three different sub-types (i.e., TBm_1, TBm_2, and TBm_3) is used for the deposits, which are massive-bedded, matrix- to clast-supported, lithic block dominant, and poorly sorted (Table 2). The facies displaying planar- to undulatory-bedded, ash-rich matrix, ash to lapilli-dominant juvenile and lithic clasts, moderately to well-sorted deposits are called ash–lapilli tuff (AT) with two sub-types (AT_1 and AT_2). The lapilli tuff (LT) is used for the clast-supported (lapilli-size) and juvenile-rich deposits (Table 2). In addition, the lithic-rich layers emplaced as a few cm thick lenses are called TBm_{lens} (Table 2).

Samples from unconsolidated beds of each maar were dried and sieved from −4 to 4 φ with 1 φ intervals ($\varphi = -\log_2 d$, where d is particle size in mm). After washing the samples in an ultrasonic bath and drying them, clasts sizes down to 2 φ (250 μm) were analyzed for componentry by counting 300 clasts from each layer under the binocular microscope, except for some beds, including clasts with fine ash coating. The calculated parameters (e.g., mode, median, sorting, and kurtosis; Inman, 1952) of each sieve analysis are given in Supplementary Data S1.

Scanning electron microscopy and density measurement

The representative maar juveniles (scoria for İcik maar, and pumice for felsic maars, except for Kalecitepe) with a grain size of 4–8 mm were selected and cleaned with chemical solutions (e.g., acetone). After drying, they were stuck to mounts and gold-coated. Secondary electron images of maar juveniles were acquired using an SEM (JEOL-JSM-7600F) at the research laboratory of Muğla Sıtkı Koçman University (Turkey) with a beam energy of 15 keV and a working distance of 8 mm.

The bulk densities of maar juveniles were measured using a helium pycnometer at the Central Laboratory of Middle East Technical University (Ankara, Turkey). The densities of each

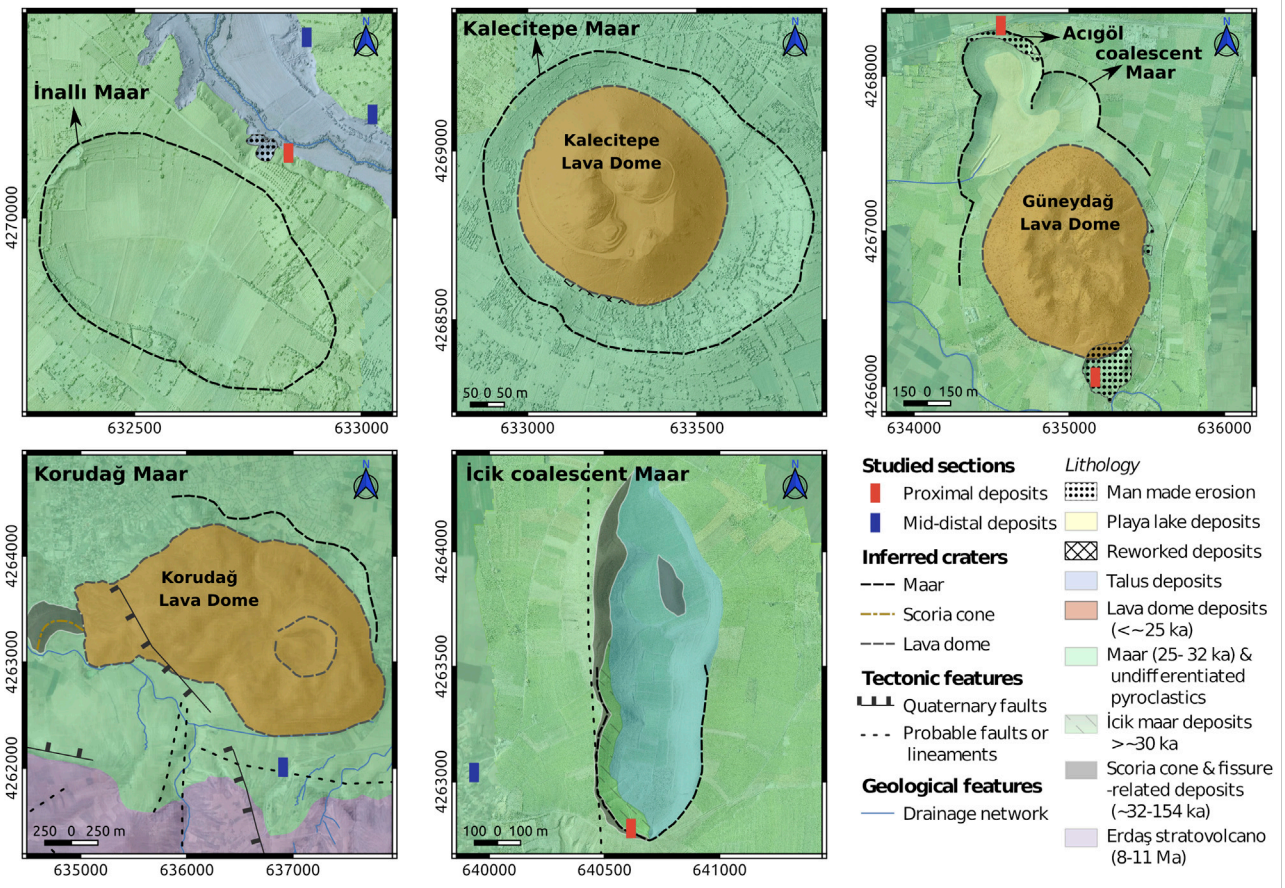

FIGURE 2
Geological maps of studied maars and adjacent monogenetic volcanoes. The shaded images in the backgrounds are high-resolution (6–13 cm/px) drone-based digital surface models and orthomosaics, except for the Korudağ maar, where 30 m-resolution digital elevation models (ALOS 3D World) and Google Earth images were used. References for ages and faults are the same as those in Figure 1.

juvenile represent the average value of six measurements with a precision between 0.0002 and 0.0007 g/cm^3 (Supplementary Data S2).

The representative juvenile clast morphologies of each maar were examined both at macroscopic (hand specimen) and microscopic scale (thin section, secondary, and back-scattered images) to determine the shape and textural differences among the clasts (microvesicular, expanded, tube-like; Polacci et al., 2003). The basic image processing stages in Image J software (Rasband, 2006) are applied to the back-scattered SEM images of juvenile clasts to estimate the vesicle contents. After performing thresholding and basic image adjustments (e.g., contrast and brightness), the images are converted to binary. The volume percentages of black-colored vesicles are calculated by dividing their total area by those of a binary image.

Petrographical and geochemical analyses

The fresh (unaltered) and representative maar juveniles (scoria for İcik maar, and pumice, perlite, and obsidian for felsic maars, except for Kalecitepe) and a few lithics were selected for further petrographical and geochemical analysis. Polished thin sections were prepared in the laboratories of both Muğla Sıtkı Koçman University (Turkey) and the University of Geneva (Switzerland). Petrography was performed to determine the mineral assemblages and textural characteristics of the studied maar volcanics.

Major and minor element compositions of mineral (only for İcik maar) and glass (only for felsic maars, except for Kalecitepe) of maar juveniles were measured on carbon-coated polished thin sections using an electron probe micro-analyzer (EPMA; JEOL 8200 superprobe) at the University of Geneva, equipped with five wavelength-dispersive spectrometers. We used an accelerating voltage of 15 keV. For mineral analysis (only valid for İcik maar), the beam current was set at 20 nA, and we used a defocused beam of 3 μm to acquire transects or points (i.e., core, mantle, and rim) and capture the compositional variation in the analyzed minerals. For the glass measurements of maar pumices, the beam current was

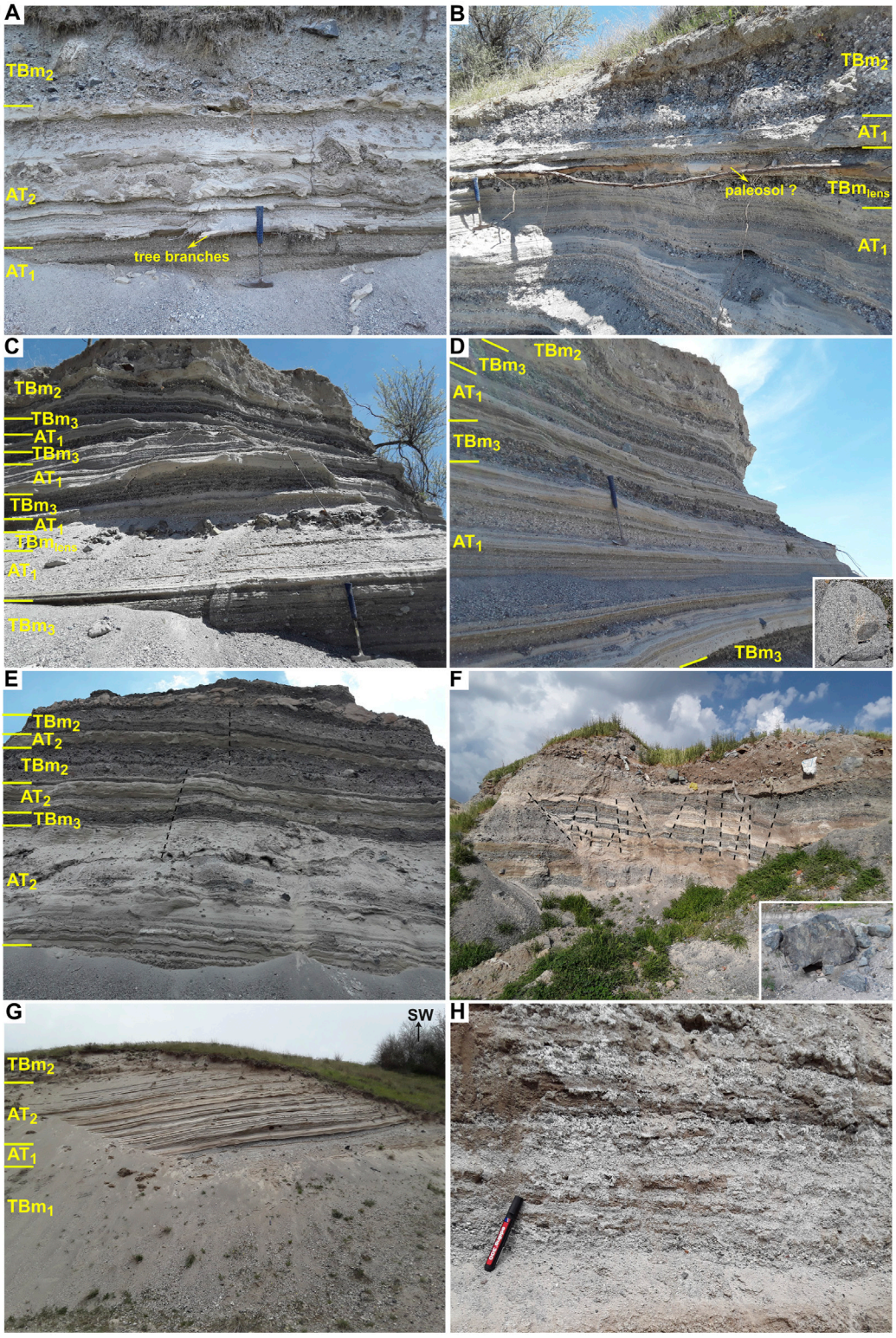

FIGURE 3
Field characteristics of the felsic maars; **(A)** the proximal and **(B)** distal (~1 km away from the maar crater) deposits of İnallı maar. **(C and D)** The proximal outcrops of Acıgöl maar with a close-up view of free lithic granite block found around the deposit. **(E and F)** The pyroclastic deposits are exposed in the southern parts of Acıgöl maar, which are possibly deformed by the post-emplacement of the lava dome (dashed black lines). The free ophiolite blocks (~1 m in length) are found around the deposit. **(G and H)** The mid-distal deposits of Korudağ maar. The close-up view in **(H)** represents the AT_1 facies. The sizes of the hammer and board marker are 40.7 cm and 12.3 cm, respectively.

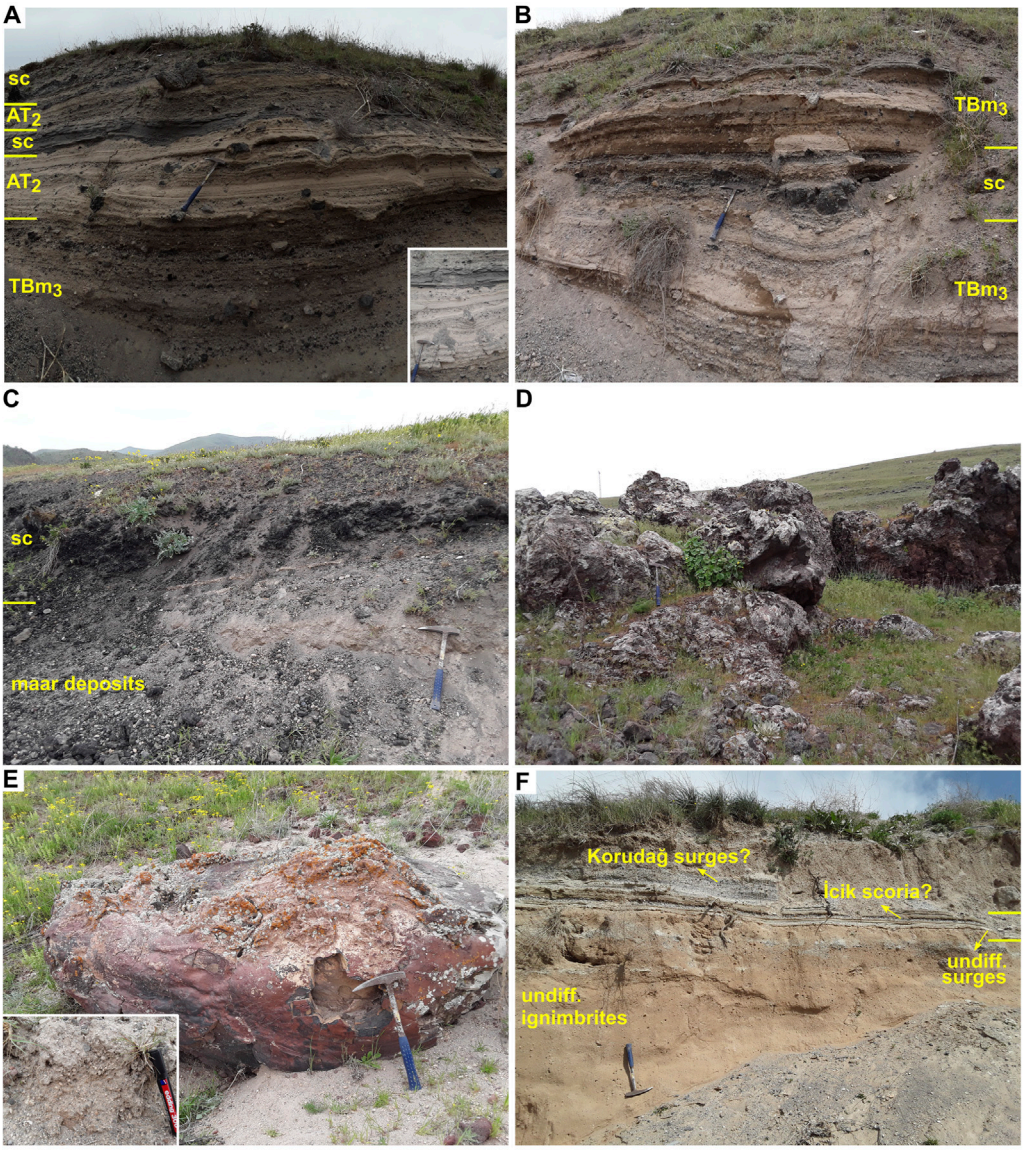

FIGURE 4
General field observations of İcik maar; **(A and B)** The upper sections of the studied maar deposits display ballistically emplaced rhyolitic lithic blocks (up to 40 cm). Inset image shows the surge deposits overlaid by gray-colored scoria-cone deposits. **(C)** The lower parts of the maar deposits intercalated with possibly syn-formational scoria cone-derived agglomerates. **(D)** Post-emplacement of scoria cone-related lava flows topping the maar deposits. **(E)** Blocky lava flows and breadcrust bombs from pre-maar activity with a close-up view of the ground deposits within the northern part of the İcik crater consisting of pumice and obsidian clasts. **(F)** The mid-distal deposits of intercalated scoria cone-related lapilli fallouts and maar deposits. The sizes of the hammer and board marker are 40.7 cm and 12.3 cm, respectively.

decreased to 6 nA, and a defocused beam of 10–20 μm was used depending on the size of the glass pools. Counting times on the peak and background were set to 30 and 15 s, respectively. The exceptions were Na and K, which are highly mobile under the electron beam, and were analyzed first and with shorter counting times (20/10 s on peak/background). We used appropriate natural minerals and glasses as standard materials.

Whole-rock geochemical analyses of 16 samples consisting predominantly of maar juveniles were performed at ACME Analytical Laboratories Ltd. (Canada) following their standard analytical and sample preparation procedures (LF 202). Major element compositions were determined using an inductively coupled plasma-atomic emission spectrometer (ICP-AES) after fusion with $LiBO_2/Li_2B_4O_7$, while trace and rare-earth elements were determined using an inductively coupled plasma-mass

spectrometer (ICP-MS) after acid decomposition (5% HNO_3). Major element concentrations were normalized on a loss-on-ignition (LOI) free basis for geochemical interpretations.

Results

Field and depositional characteristics

All studied maars have well-exposed deposits to investigate the depositional characteristics and sample for further analysis (Figure 2). The only exception is the Kalecitepe maar, which includes reworked volcano-sedimentary deposits exposed in the southern parts of the lava dome with evidence of broken Neolithic components and fossil traces (not shown). The locations of the representative stratigraphic sections of the studied maars are shown in Figure 2. The apparent thickness of the unconsolidated maar deposits varies between 3 m (e.g., İnallı) and 9 m (e.g., İcik) (Table 1). While both proximal (3 m-thick) and mid-distal (1–1.5 m-thick) deposits were observed in İnallı maar, Korudağ maar only has a mid-distal sequence (~1 km away from the crater center; Figures 2, 3). In the Acıgöl maar, the deposits cropped out in the northwestern and southeastern regions were examined (Figure 2). İcik maar also has both proximal (9 m-thick) and mid-distal (15 cm-thick) deposits, which are found in the southwestern parts of the maar and near the İcik village (~500 m away from the maar crater), respectively (Figures 2, 4). Here, we described the characteristics of each maar of the Acıgöl caldera.

İnallı maar

The 3 m-thick proximal deposit exposed in the northeastern flanks of the maar crater (Table 1; Figure 2) consists mainly of four distinct lithofacies (Figures 3A and B; Figure 5). These facies are distinguished based on sedimentological characteristics (e.g., bedding types, stratification, and contacts). There is no paleosol observed in this proximal deposit (Figure 3A), whereas the outermost mid-distal outcrop bears a thin (~ 5 cm) paleosol layer (Figure 3B). The proximal section can be divided into lower (TBm_1, AT_1) and upper units (AT_2, TBm_2):

- TBm_1 is a massive-bedded, lithic block-bearing unit that covers the first ~1.5 m of the stratigraphy (Figure 5). The lithics are mostly deformed/weathered granitoids with rare amounts of ophiolites and ignimbrite-derived pinkish pumice lapilli, while the juveniles are predominantly sub-angular to sub-rounded pumice, perlite, and obsidian clasts. The average maximum size of the lithics and juveniles (pumices) is 20 cm and 10 cm, respectively, while the juvenile obsidians and perlites are medium to coarse lapilli-sized. The lapilli-size materials are mostly represented by juveniles, while the finer sizes are dominantly free crystals and fragmented particles (mostly biotite and feldspar), mostly derived from crustal lithics (Figure 6). The median grain size (excluding the large lithic blocks >64 mm) measured by the sieve analysis is −2.29 ϕ (i.e., medium lapilli range; Figure 6 and Supplementary Data S1). The ash-rich matrix is moderately well sorted (σ = 1.49; Figure 6). The sedimentary structures are represented by impact sags resulting from the deformed granite blocks (up to 20 cm). The lower contact of this unit is not observed due to the presence of talus deposits. In addition, the thickness of this unit gradually decreases toward the mid-distal locations.
- AT_1 is a planar bedded unit displaying stratified, very well-sorted (σ = 1.22), gray to beige pyroclastic deposits (Figures 3A and B, Figure 5, and Figure 6). It consists of intercalated thin ash and a few cm-thick lapilli-rich layers. The lithics (ophiolite, ignimbrite-derived pinkish pumices, and granites) are rather limited (~15%) compared to the juveniles (~35%; pumice, perlite, and obsidian) in coarse grain fraction, while the free crystals and fragmented particles (derived mostly from lithics) are more dominant in finer fraction (up to 45%; Figure 6). The average maximum grain sizes of lithics and juveniles measured in the field are 4.1 cm and 3.4 cm, respectively. The median grain size value is measured as −0.17 ϕ (i.e., the range of very coarse ash; Figure 6 and Supplementary Data S1).
- AT_2 unconformably overlies the AT_1 with a more chaotic stratification displaying large granite lithics transported within an ash-rich matrix (Figure 3A). The 50 cm-thick sequence also exhibits indistinct chute and pool lamination due to the gravitational effects of large lithics over the underlying ash matrix (Figure 3A). The juveniles are limited to the ash-size particles, while the lithics are represented by granite blocks with an average maximum size of 14 cm (Figure 3A). This unit ends with a 10 cm-thick ash-rich layer, including medium-lapilli-sized obsidian and lithic clasts (Figure 3A). In addition, it laterally continues through the northeastern parts of the crater (~500 m) and disappears in distal outcrops (Figure 3B).
- TBm_2 is the uppermost unit (~ 40 cm) consisting predominantly of juvenile obsidian blocks (up to 40 cm) found within the ash- to the lapilli-rich matrix (Figures 3A and B and Figure 5). The massive bedded unit without any sedimentary structure also includes lapilli-sized, sub-angular to sub-rounded juvenile pumice (~ 5 cm) and perlite (~ 4 cm) clasts within a moderately sorted matrix (σ = 1.74; Figure 6). The juvenile-rich (~85%) unit has a median grain size of −2.41 ϕ (i.e., medium lapilli range; Figure 6). The lithics represent a small percentage (~10%; e.g., lapilli- to block-sized granites). Through the mid-

distal locations, the grain size of the volcanics gradually decreases (Figure 3B).

Kalecitepe maar

Kalecitepe is a compound maar mostly occupied by the post-emplacement of a rhyolitic lava dome (Table 1, Figure 1C, and Figure 2). The maar deposits are not exposed, and the only visible deposits are the ash-sized tephra found along the inner walls of the crater, which have been used for cultivation (Supplementary Figure S1). In addition, the crater is partly filled by mixed or reworked deposits, including broken pieces of fossil traces and Neolithic remnants (Supplementary Figure S1).

Acıgöl maar

Acıgöl is a coalescent maar formed by at least three craters: one of which is occupied by a lava dome (Table 1, Figure 1C, and Figure 2). The ejecta rings are exposed in the northwestern and southeastern parts of the maar crater walls (Figure 2). The northwestern deposit with a thickness of ~5 m displays four main lithofacies (TBm_3, AT_1, F_1, and TBm_2) distinguished by sedimentological features (Figures 3C and D and Figure 5). The juveniles are pumice, perlite, and obsidians that are generally lapilli- to block-sized. The lithics of granite, andesite, ophiolite, and undifferentiated crustal rocks mostly have block sizes, but some of them can be up to a few meters (Figures 3C–F). The identified lithofacies are described in the following text from the lower to upper parts of the stratigraphy:

- TBm_3 is a crudely stratified unit including lapilli- to block-sized (up to 11 cm) heterolithic clasts (Figure 3C; Figure 5). This unit is partly clast-supported within a limited dark gray ash matrix that differs from the TBm_1 described in İnallı maar, with intercalations of well-stratified ash-rich thin layers. There is no sedimentary structure, and the juveniles are limited to a few lapilli-sized obsidian and pumice clasts. The sub-angular lithics are predominantly dark-colored andesites, with some granites, ophiolites, and undifferentiated lithics. From field measurement, the average maximum size of the lithics is 9.5 cm. Through the upper parts of the stratigraphy, the dark-green ophiolite lithics become more abundant.
- AT_1 is a few meter-thick (~2 m) unit, exhibiting planar-bedded, partly clast-supported, and well-stratified pyroclastic deposits, which are partly intercalated with ash-rich thin layers (Figure 3D; Figure 5). The moderately to well-sorted (σ = 1.32–1.94) unit has a median grain-size distribution of coarse to very coarse ash (-0.05–0.95 ϕ; Figure 6). The juvenile fraction, composed mostly of pumices (~40%), is larger compared to the lithics (~15%), which are andesites, ophiolites, granites, and ignimbrite-derived pinkish pumice clasts. However, the finer grains are dominated by free crystals (e.g., feldspars and mica minerals) and fragmented particles (e.g., broken obsidians and perlites). The intercalation of AT_1 and TBm_3 facies completely covers the stratigraphy until the last ~50 cm (Figure 5). In the middle parts, there is also a ~40 cm-thick layer (TBm_{lens}) exhibiting an accumulation of various types of block-sized lithics (Figure 3C).
- TBm_2 represents the last ~50 cm of the stratigraphy and comprises predominantly block-sized (up to 15 cm) juvenile pumice, perlite, and obsidians within a lithic-poor ash matrix. As described in the İnallı maar, this massive bedded unit is significantly rich in juveniles (~ 85%) compared to lithics (~10%). There is a thin layer of clast-supported, pumice-rich deposit ($\mathbf{LT_1}$) at the base of the TBm_2 that unconformably overlies the AT_1 facies.

Another exposed section of pyroclastic deposits (~10 m) is found in the southeastern parts of the maar through the outer flanks of the Güneydağ lava dome (Table 1 and Figure 2). We could not sample the stratigraphy due to the weak stability of the outcrop, but we distinguished three main lithofacies in the pyroclastic sequence (Figures 3E and F) starting from the bottom:

- AT_2 is a moderate to well-stratified, undulatory-bedded unit interstratified with thin ash-rich layers (Figure 3E and Figure 5). The thickness of the unit varies from a decimeter to a few meters (~4.5 m). The small-scale dune structures are especially present in the upper sections of the stratigraphy, where the matrix color changes from white to light brown. The impact sags and pinch and swell structures are also observed (Figure 3E). The average clast size of juveniles and lithics (mostly andesites and ophiolites) is coarse ash to medium lapilli.
- TBm_3 is a crudely stratified, lithic-rich (mostly andesite and ophiolites) unit. The unit is clast-supported with less amount of dark-colored matrix. The intercalated thin ash-rich layers in some levels result from stratification. The sub-angular lithics have an average maximum size of 8.5 cm, while the juvenile pumices and obsidians, which are rather rare, are mostly lapilli in size.
- TBm_2 is a few decimeter-thick, massive-bedded unit containing sub-angular to angular block-sized (up to 25 cm) juvenile pumice/perlite and obsidian clasts. The lithics (e.g., andesite and ophiolite) are very poor and limited to lapilli size in the ash matrix. This unit is intercalated with the AT_1 facies that display dune structures and partly impact sags with the ash-rich matrix (Figure 3E).

The stratigraphy is topped by block-sized (up to 50 cm) irregular Kumtepe ignimbrite deposits (Figure 3E; Figure 5). In addition to the facies characteristics, the outcrops here display

various structural features (e.g., growth faults, antithetic-synthetic faults, and recumbent folds) (Figures 3E and F). Similar to the outcrop in the northwestern part of the maar, there are also meter-sized free lithic ophiolite blocks (Figure 3F).

Korudağ maar

The Korudağ maar is located at the northeastern edge of the NW-SE alignment of felsic maars and adjacent lava domes (Table 1, Figure 1C, and Figure 2). It has accessible outcrops in both northern (Türkecan et al., 2004) and southern (this study) parts of the maar. Some possible distal deposits are also found in two different locations, near the İcik village (Türkecan et al., 2004) and as a ground deposit within the İcik maar crater (this study). The ejecta ring of the maar is almost completely deformed by the emplacement of a lava dome complex, which is faulted in the western parts (Figure 2). We investigated the mid-distal deposits exposed in the southern parts of the Korudağ maar (Figures 3G and H). The ~6 m-thick maar deposits consist predominantly of four main lithofacies (TBm_1, AT_1, AT_2, and TBm_2; Figure 5):

- TBm_1 is a massive-bedded unit displaying lithic blocks within the ash-rich matrix. These lithics (mostly andesite and granite) have an average maximum size of 24 cm. In addition, coarse lapilli-sized (up to 5.5 cm) juvenile pumices and obsidians are characteristic. The depositional features are not well observed due to the talus deposits that mostly cover the unit (Figure 3G). The ash-rich matrix with the median grain size of −0.21 ϕ (very coarse ash range) exhibits moderate to poor sorting (σ = 1.93; Figure 6). Despite the limited amounts of coarse lapilli to block-sized juveniles, the componentry analysis reveals that the ratio between juveniles (42%) and lithics (45%) is comparable. The finer sizes (< 1 ϕ) are dominated by free crystals and broken lithic fragments (Figure 6).
- AT_1 is a planar-bedded and well-stratified unit including lithic-rich (mostly andesite and granite) lenses (TBm_{lens}) partly observed in some levels (Figures 3G and Figure 5). The unit is enriched in ash-sized material (Figure 3H), predominantly juveniles (45%) and free crystals (30%) including deformed country rocks (Figure 6). The lithics are partly differentiated in the componentry works as dark-colored rocks and granite fragments. The moderately sorted (σ = 1.65) unit has a median grain size of 0.93 ϕ (coarse ash range; Figure 6).
- AT_2 is planar to an undulatory-bedded unit that displays good stratification due to the intercalation between ash and lapilli-rich layers (Figure 3G). This unit differs from AT_1 by its sedimentary structures, such as low-angle and climbing dunes (Figures 3G; Figure 5). The medium-lapilli-sized juveniles are measured in the field, but the average median grain size is 0.65 ϕ (coarse ash range). The unit is poorly sorted (σ = 2.06). The juvenile ratio (47%) is significantly higher than the lithics (18%), but the free crystals and fragmented lithics are especially dominant in the finer sizes (Figure 6). This unit covers a significant portion of the stratigraphy (~2.5 m) and partly includes intercalated lithic-rich lenses (TBm_{lens}).
- TBm_2 is the uppermost unit with typical juvenile blocks consisting of pumice, obsidian, and rare perlite. The juveniles are generally sub-angular and can reach up to 30 cm in size (obsidians). A minor proportion of lithics (10%) is mostly found within the matrix as lapilli clasts (with rare granite blocks), whereas the juveniles are predominant (up to 90%). The matrix is moderately sorted (σ = 1.83) with a median grain size of −2.83 ϕ (medium lapilli range; Figure 6).

İcik maar

İcik is another coalescent maar found toward the central parts of the Acıgöl caldera and formed along an NNW-SSE trending fault (Table 1, Figure 1C, and Figure 2). There are at least two nested maar craters where the northern rim is deformed by the syn- or post-formational scoria cone (Figure 2). The proximal maar deposits are exposed in the southern parts of the crater wall, exhibiting a whole spectrum (~9 m thick) of the subsurface deposits (Figures 4A–C). The juveniles are mostly represented by less vesicular scoria clasts and cauliflower bombs, whereas the lithics include rhyolites, andesites, lapilli-sized pumice and obsidians, and undifferentiated crustal rocks. In addition, more vesicular scoria clasts compared to maar scoria are considered to be derived from the adjacent scoria cone, together with the agglomerates described in some layers. We have differentiated the following three main maar lithofacies (TBm_3, AT_1, and AT_2) in stratigraphic order:

- TBm_3 is a massive bedded, crudely stratified, lithic-rich unit that occupies the first half of the stratigraphy (Figures 4A and C and Figure 5). The lithics in the lower sections are represented by lapilli-sized rhyolites, andesites, obsidians, and undifferentiated crustal rocks. However, the lithic size (up to 20 cm) increases through the upper sections (Figures 4A and C). The juvenile amount is lower (~35%) compared to the lithics (65%) and represented by the scoria lapilli and a few cauliflower bombs (~ 7 cm). There is no sedimentary structure, and the lithic blocks are generally embedded within the poorly sorted matrix (σ = 2.37–2.53) that has a median grain size of -1.21–0.08 ϕ (coarse ash to fine lapilli range; Figure 6).
- AT_2 is an undulatory-bedded unit consisting of intercalated thin ash- and lapilli-rich layers (Figures 4A and B and Figure 5). There are some cauliflower bombs (~12 cm) (Figure 4A). In addition, the common lithic blocks (predominantly rhyolite) result in the formation of impact sags and scour channels (Figures 4A and B). The

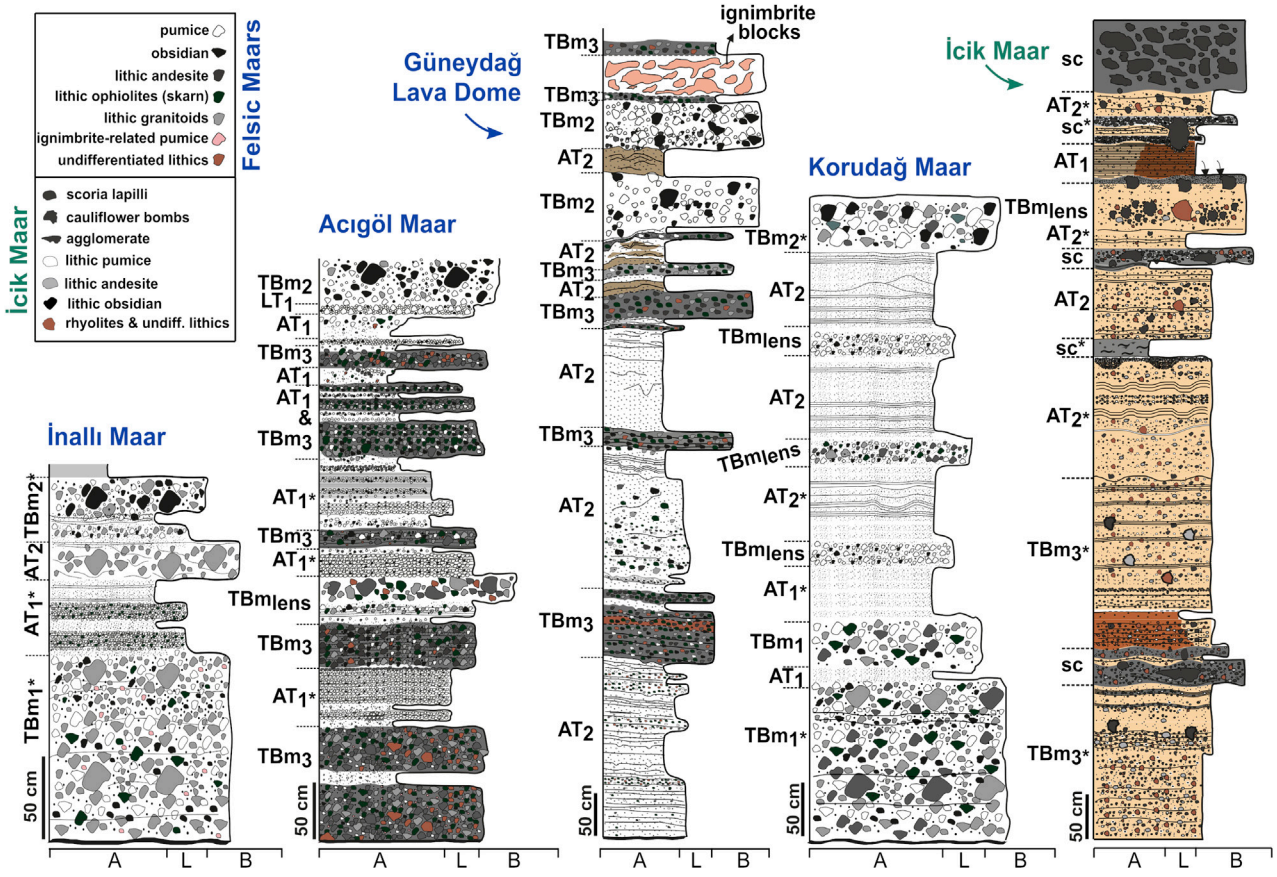

FIGURE 5
Representative stratigraphic sections of the studied maar deposits. The lithofacies abbreviations are provided in the text. * denotes the facies sampled for sieve and componentry analyses.

anti-dunes are also characteristic structures observed in the ash-rich layers (Figure 4A). The average maximum size of these lithics is 35 cm. The lithic ratio (48%) is slightly higher than those of the juveniles (45%; Figure 6). The median grain size of the poorly sorted matrix (σ = 2.47) is −1.34 ϕ (fine lapilli range) and becomes coarser in the upper sections (−2.39 ϕ), where there is a lithic-rich layer (TBm_{lens}) emplaced as a lens (Figure 6).

- AT_1 is a well-stratified, planar-bedded unit including fine- to medium-lapilli scoriae and accessory lithics (e.g., pumice and rhyolite). Small-scale impact sags are also observed. The 50 cm-thick unit, which is only observed close to the top of the stratigraphy, is partly eroded probably due to the infiltration of surface runoff. Hence, the ash-rich matrix has a muddy-like appearance.

Along the stratigraphy, some distinct layers comprising agglomerates, vesicular scoria and bombs, and gray-colored muddy fine ash are present (Figure 4B and Figure 5). These layers called "sc" are generally intercalated with the maar deposits, which are, together, mantled by the blocky lava flows at the top of the stratigraphy (Figures 4B and C and Figure 5). These layers are all dominated by scoria cone-related volcanics consisting of both coarse ash- (0.88 ϕ) and coarse lapilli-sized (−4.10 ϕ) grains (Figure 6). In addition, blocky lava flows with large breadcrust bombs (~1.5 m) are also observed within the crater base (Figures 4D and E), together with the lapilli-sized lithic pumices and obsidians. Figure 4F illustrates the possible mid-distal deposits (~ 5 cm) of İcik maar or adjacent scoria cone. This clast-supported, scoria lapilli-rich deposit is intercalated with the undifferentiated, well-stratified pumice and obsidian-rich deposits (Figure 4F).

Juvenile clast morphology and density

Felsic maars (Inallı, Acıgöl, and Korudağ)

The macroscopic and microscopic observations display a large variability of clast morphologies among the juvenile pumices of each felsic maar (Table 1). İnallı maar pumices, for example, are predominantly elongated and tube-like

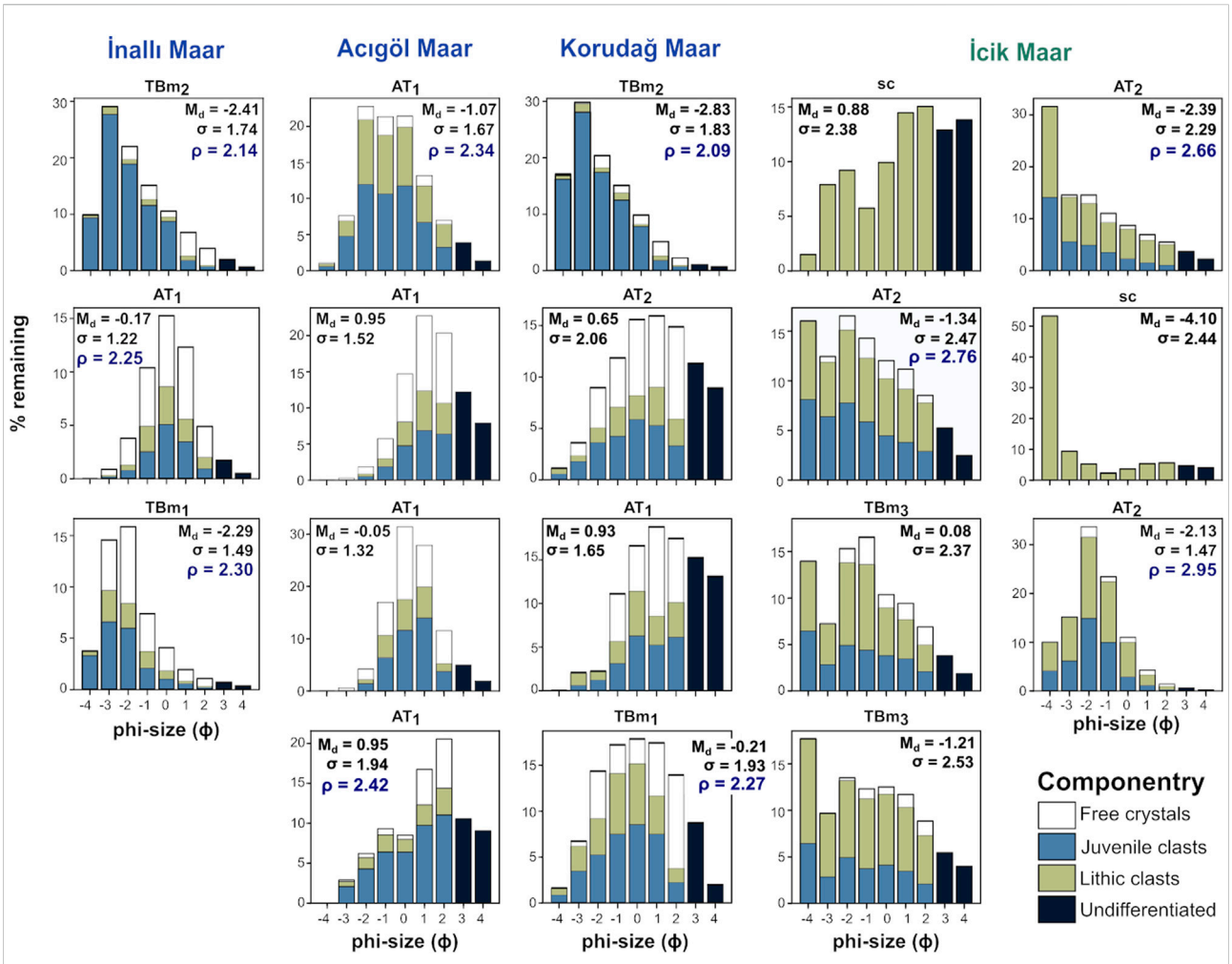

FIGURE 6
Grain-size distributions (in phi-scale) and juvenile average bulk densities (ρ in g/cm^3) of the studied maar deposits. Md_Φ: median grain size; σ_Φ: sorting.

(Figure 7A). The SEM and BSE images (Figure 7B and Supplementary Figure S2) indicate elongated and coalesced vesicles in the tube pumices of İnallı maar. In Acıgöl maar, the sub-angular pumices (outer shape) are slightly elongated (Figure 7C), but there are both dense and vesicular pumices (Figure 7D and Supplementary Figure S2). The vesicles are sub-spherical, and the smaller ones are generally coalescent. The pumices in Korudağ maar are both expanded and equant with a sub-rounded outer shape (Figure 7E). There are some tube-like vesicles visible under the SEM imaging (Figure 7F).

The bulk densities of juvenile clasts are measured for each maar along the stratigraphy (Figure 6 and Supplementary Data S2). The densities generally decrease through the end of the stratigraphy where the TBm_2 facies are deposited (Figures 5 and 6). The average decrease in the density from the lower to upper sections of the stratigraphy is approximately 10% (Figure 6), with the pumices of TBm_1 in İnallı maar having an average density of 2.30 g/cm^3, whereas the pumices in the uppermost facies (TBm_2) have an average density of 2.14 g/cm^3 (Figure 6). The pumices of Acıgöl maar have comparably higher densities (2.34 and 2.42 g/cm^3; Figure 6). The densities of Korudağ pumices are comparable with those of İnallı maar (2.09 and 2.27 g/cm^3; Figure 6 and Supplementary Data S2).

Mafic İcik maar

There are two types of scoria clasts identified in the İcik maar, which are less (~ 40 vol%) and high (~60 vol%) vesicular scoriae (Supplementary Figure S3). Both have sub-angular to sub-rounded shapes, but equant scoriae, including sub-spherical coalescent vesicles, which are partly filled by secondary minerals, are more common (Figures 7G and H and Supplementary Figure S3). The bulk densities measured along the stratigraphy are mostly scattered

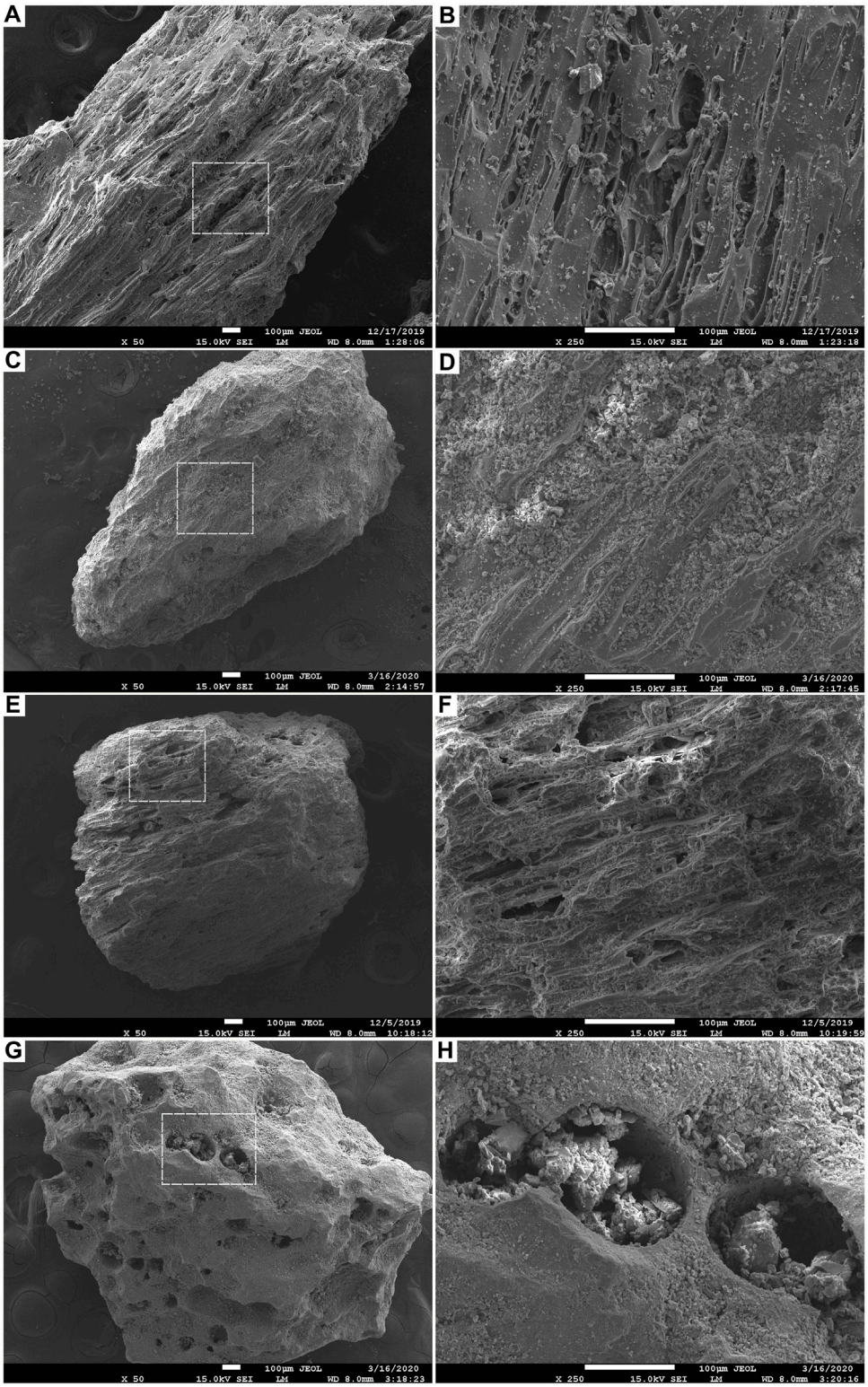

FIGURE 7
SEM images of **(A and B)** the juvenile tube pumice lapilli of İnallı maar and its close-up view; the elongated and coalesced vesicles are more common. **(C and D)** Acıgöl maar fine-lapilli and its detailed view; the tube pumices are generally dense. **(E and F)** The pumice lapilli of Korudağ maar and its close-up view; the pumices are mostly expanded together with less amount of slightly elongated vesicles. **(G and H)** The scoria lapilli of İcik maar; the equant clasts, including sub-spherical to spherical vesicles.

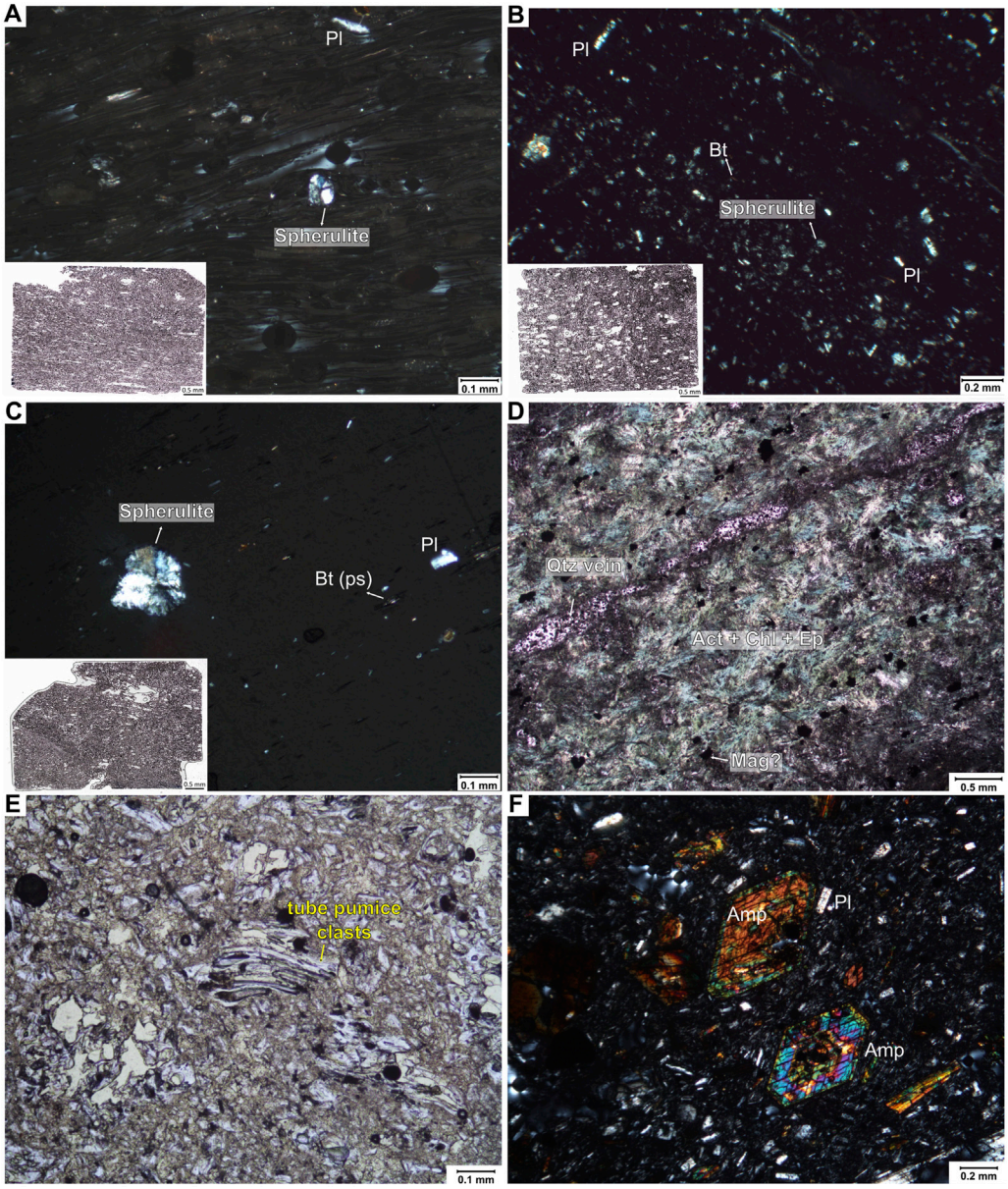

FIGURE 8
Photomicrographs of juvenile and lithic clasts of felsic maars. **(A)** The cross-polarized light view of a pumice clast of İnallı maar with a few plagioclases (Pl) microlites and spherulites. The inset shows the scanned thin section of the pumice clast in a plane-polarized light view. **(B)** The banded obsidian of Acıgöl maar, including biotite (Bt) and plagioclase microlites with a few spherulites in a glassy matrix. The inset displays the scanned thin section of a pumice clast, including expanded vesicles. **(C)** The banded obsidian of Korudağ maar displaying plagioclase microlites, biotite pseudomorphs, and spherulites. The inset shows the scanned thin section of a tube pumice clast with elongated vesicles. **(D)** The altered lithic diabase from Acıgöl maar. **(E)** The lithic volcanic breccia of Acıgöl maar consists of various pumice clasts, including tube pumices. **(F)** Andesitic lithic found in the Korudağ maar deposits, including euhedral amphibole phenocrysts. Abbreviations: Qtz, quartz; Mag, magnetite; Amp, amphibole; Act, actinolite; Chl, chlorite; Ep, epidote.

(Figure 6 and Supplementary Data S2). The scoriae in the lower section have an average density of 2.76 g/cm^3, which decreases to 2.66 g/cm^3 toward the top (Figure 6). However, the density again increases in the uppermost maar deposits (2.95 g/cm^3; Figure 6).

Petrography

Felsic maars (Inallı, Acıgöl, and Korudağ)

The juveniles of felsic maars, which are mostly aphyric, have very similar petrographical features (Table 1 and Figures 8A–C).

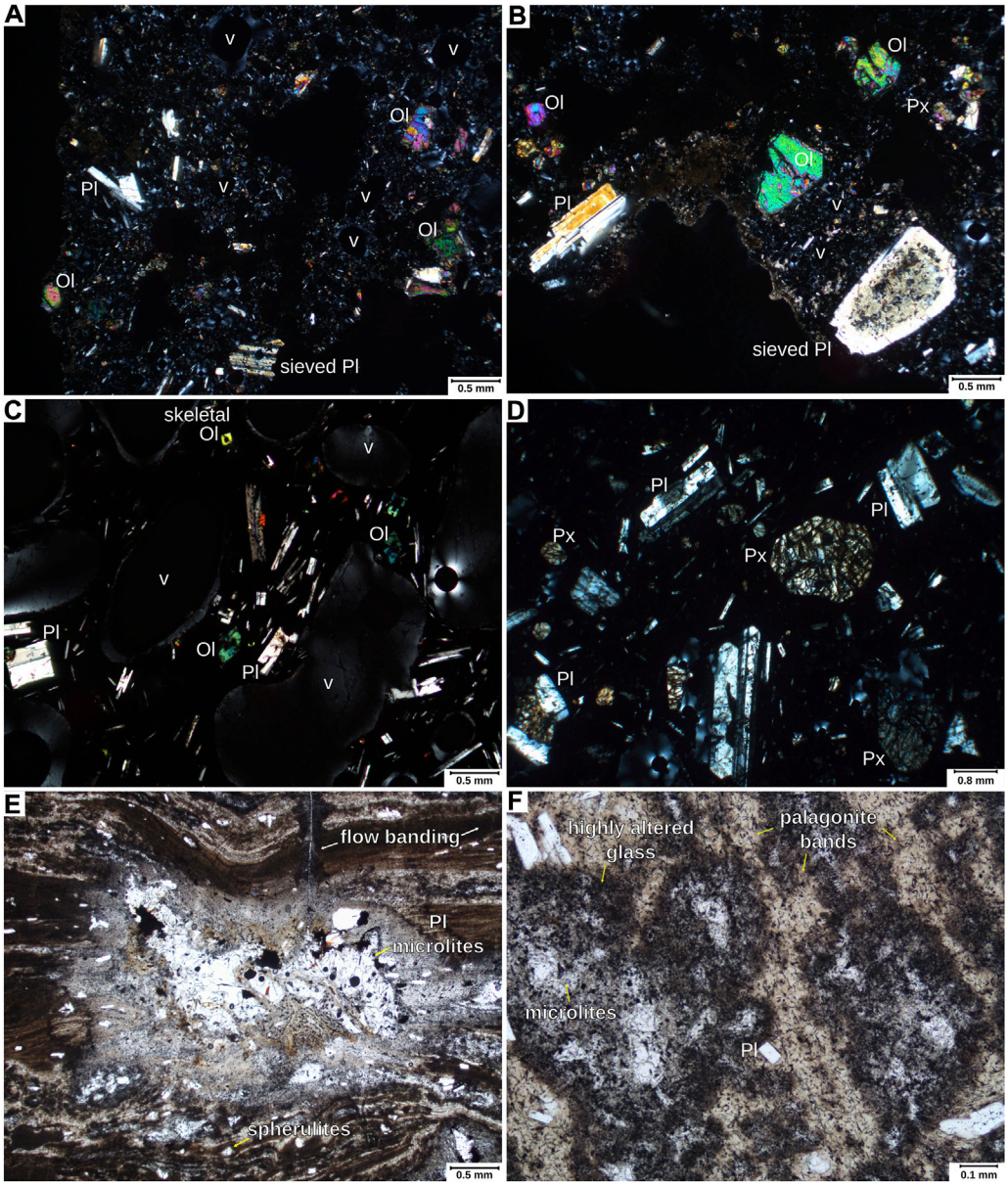

FIGURE 9
Photomicrographs of juvenile and lithic clasts of mugearitic İcik maar. **(A and B)** Maar scoria consisting predominantly of altered and fresh plagioclases (Pl) and skeletal olivines (Ol). **(C)** The highly vesicular (v) vitrophyric bomb, including olivine microlites and plagioclase microphenocrysts. **(D)** The andesite lithic displaying euhedral pyroxene (Px) and plagioclase phenocrysts. **(E)** The lithic-banded rhyolite, including plagioclase microlites and spherulites. **(F)** The altered rhyolite with palagonite bands and vuggs, including plagioclase and secondary quartz microlites.

The tube pumices of İnallı maar have only a few plagioclase and biotite microlites, together with rare spherulites, set in a glassy matrix (Figure 8A). The banded and partly hypocrystalline obsidians of Acıgöl maar have feldspar and biotite microlites with spherulites (Figure 8B). However, the pumices of Acıgöl maar are nearly aphyric (the inset of Figure 8B). Korudağ obsidians also display banding with a microlite-bearing groundmass consisting of plagioclase, pseudomorphic biotites, and spherulites (Figure 8C). The partly welded pumices (inset of Figure 8C) are nearly aphyric, similar to other felsic maars.

The petrography of the lithics found in the felsic maar deposits is shown in Figures 8D–F. The crystalline basement rocks, such as granites (not shown), the altered ophiolitic rocks (probably diabase), and the andesites, are the most common lithics. The mineral assemblage of altered ophiolite is actinolite, chlorite, epidote, and oxides (e.g., magnetite; Figure 8D). The

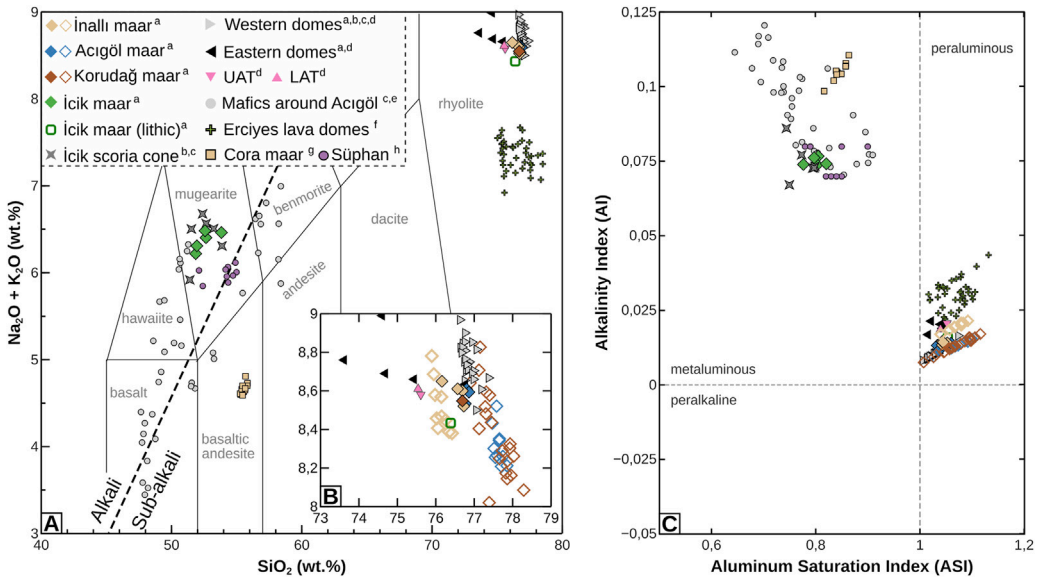

FIGURE 10
(A) Total alkalies vs silica (TAS) diagram displaying the whole-rock geochemistry of the studied maars (juveniles) and other volcanics of Acıgöl caldera and Erciyes stratovolcano. A black dashed line separates the alkali and sub-alkali compositions (Irvine and Baragar, 1971). **(B)** Close-up view of rhyolite field representing both whole-rock and glass (empty diamond symbols) geochemistry of the studied felsic maars together with other rhyolitic volcanics in Acıgöl caldera. **(C)** ASI [Al/((Ca-3.33*P)+Na+K)] vs AI [Al-(Na+K)] diagram (both in molar; Frost and Frost, 2008). [a] This study; [b] Türkecan et al. (2004); [c] Aydar et al. (2011); [d] Siebel et al. (2011); [e] Di Giuseppe et al. (2018); [f] Friedrichs et al. (2020); [g] Gençalioğlu-Kuşcu (2011); [h] Özdemir et al. (2011).

andesites have a trachytic texture with a plagioclase-dominated groundmass and microphenocrysts of euhedral amphibole and altered plagioclase (Figure 8E). Both altered and fresh rhyolites, together with some volcanic breccias, are also common. Figure 8F represents a typical example of volcanic breccia found in Acıgöl maar that includes various sizes and types of pumice clasts (mostly tube-like). In addition, some of the pumices from İnallı maar involve a few clasts of basement granites (Supplementary Figure S4).

Mafic İcik maar

The scoria clasts of İcik maar consist predominantly of olivine and plagioclase microphenocrysts with rare pyroxenes, alkali feldspars, and Fe-oxides (Figures 9A–D). There is a textural variability among the scoriae; some are hypocrystalline with low vesicularity (Figures 9A and B), while others are highly vesicular (Figure 9C). They are weakly microporphyritic within a microlite-bearing groundmass (Figures 9A–C). Olivine microphenocrysts are generally skeletal. Plagioclases are both fresh and have sieved textures in the low vesicular scoriae (Figures 9A and B), while they are all fresh with swallowtails in the high vesicular ones (Figure 9C).

The petrographic features of some lithics found in the maar deposit are illustrated in Figures 9D–F. The andesitic lithic, for example, displays a porphyritic texture with the main mineral assemblage of pyroxene and plagioclase (Figure 9D). The various types of lithic rhyolites (e.g., devitrified and palagonitized rhyolites) were observed in İcik maar (Figures 9E and F).

Geochemistry

Whole-rock and glass major-oxides

All major-element compositions of whole-rock analysis are normalized to loss on ignition-free contents (LOI; 0.2–4.7 wt%) or 100 wt% in the case of glass analysis (Supplementary Data S3 and S4). The geochemistry analyses show that the felsic maars (İnallı, Acıgöl, and Korudağ) have a rhyolitic composition with a SiO_2 range of 76.2–76.9 wt% and 75.9–78.3 wt%, respectively (Figures 10A and B and Supplementary Data S3 and S4). İnallı maar, among the felsic maars, has the least evolved glass compositions (Figure 10B). All felsic maars are peraluminous rhyolites, similar to the Holocene lava domes of Erciyes stratovolcano, with an Alumina Saturation Index [ASI; molar Al/((Ca-3.33*P)+Na+K] of 1.03–1.06 and an Alkalinity Index [AI; molar Al-(Na+K)] of 0.01 (Figure 10B). Together with the compiled data for felsic volcanics in the Acıgöl caldera (see Figure 10 for references), the alkali content (Na_2O+ K_2O wt %) tends to decrease with increasing SiO_2 (Figure 10B).

The mafic İcik maar having a mugearitic (or basaltic trachyandesitic) composition (51.9–53.8 wt% SiO_2) displays a negative trend in the TAS diagram, similar to other mafics

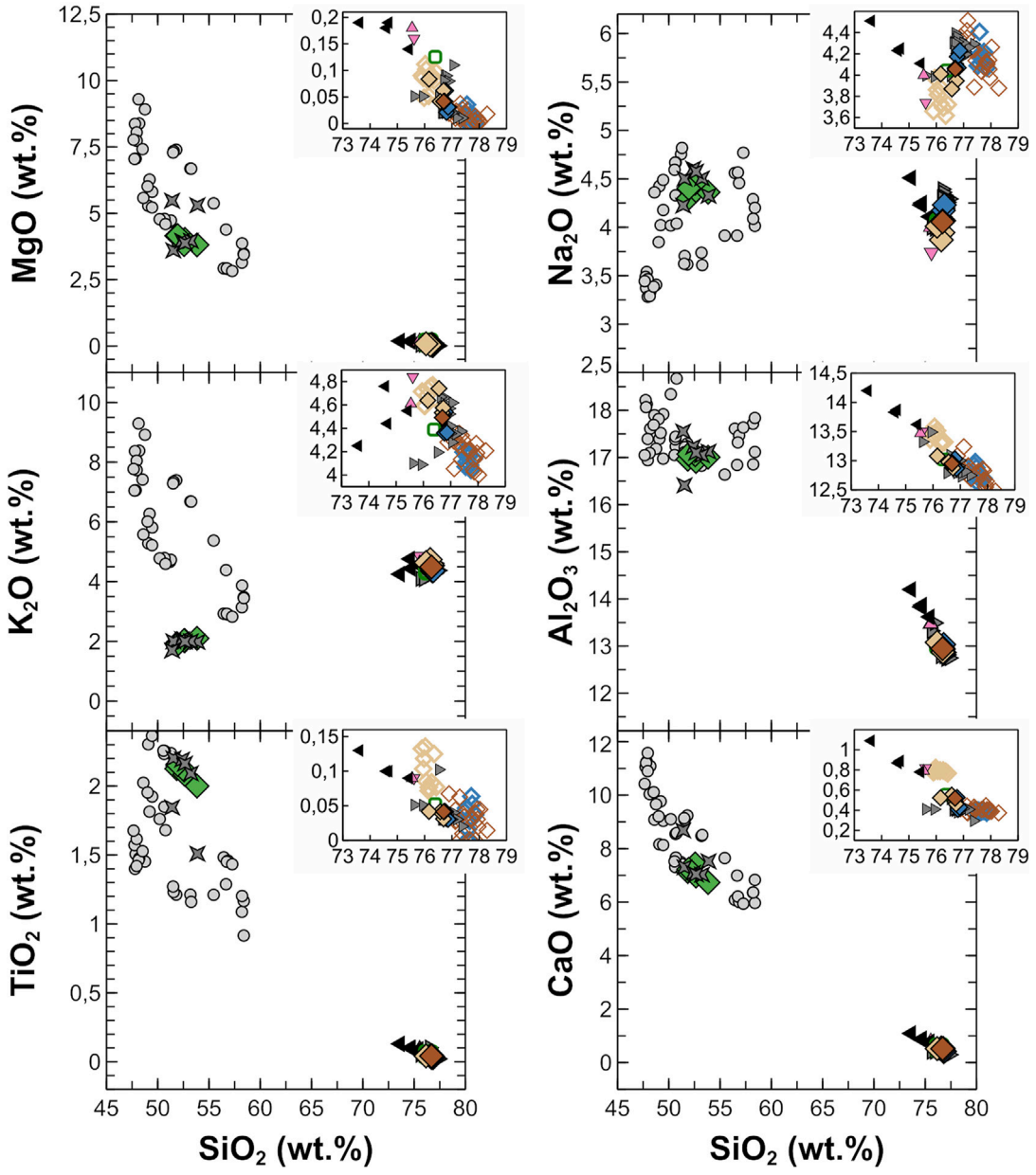

FIGURE 11
Harker diagrams for selected major oxides of studied maars and other Acıgöl volcanics. Inset images show the close-up views of rhyolite fields (empty diamond symbols representing the glass compositions; see Figure 10 for the entire symbology and related references).

around Acıgöl caldera (Figure 10A). They have slightly elevated alkali contents (Na_2O > K_2O; ~4.4 and 2.0 wt%, respectively) compared to their compositionally equivalent Cora maar (NW of Erciyes stratovolcano, Gençalioğlu-Kuşcu, 2011; Na_2O > K_2O: ~3.5 and 1.2 wt%, respectively; Figure 1B and Figure 10A). Similarly, the mugearitic Quaternary rocks from the Süphan volcano (eastern Anatolia) have almost comparable alkali compositions (Figures 10A and C; Özdemir et al., 2011). In addition, the İcik maar and scoria cone deposits, together with the Cora maar and other compiled mafics outside the Acıgöl caldera, are all metaluminous (Figure 10C; Aydar et al., 2011; Di Guiseppe et al., 2018).

Figure 11 illustrates the changes in major element compositions (both whole rock and glass) of the studied maars with respect to SiO_2 contents (i.e., Harker diagrams). İnallı maar, which plots at the lower end of the silica range, differs in its major element compositions compared to the other felsic maars. It has higher contents in most of the major elements

(K_2O, Al_2O_3, and TiO_2), whereas the Na_2O values are much lower, especially for the glass compositions (Figure 11 and Supplementary Data S3 and S4). Looking at both the whole-rock and glass compositions of the felsic maars (inset in Figure 11), a negative trend for most major elements, except for the Na_2O, can be observed with increasing SiO_2. The adjacent lava domes (i.e., western domes) have a compositional range comparable to the maars (Figure 11), with a continuous negative trend starting from the older eastern domes to the younger maars and lava dome complexes for MgO, Al_2O_3, and CaO vs. SiO_2 (Figure 11).

Major element composition of the İcik maar scoriae forms clustering (Figure 11), but a positive trend in K_2O, together with negative trends of TiO_2 and CaO with increasing SiO_2, can be observed (Figure 11). The maar scoriae compositions are also identical to the possible scoria cone-derived volcanics compiled from the literature (Figure 11). Other mafics across the Acıgöl caldera have more scattered patterns of major element compositions (Figure 11).

Mineral chemistry

The mineral chemistry analysis is performed only on the İcik maar scoriae due to the aphyric nature of the felsic maars. In line with the identified mineral assemblages of İcik maar scoriae, the major-element compositions of the olivine and plagioclase microphenocrysts, together with a few Fe-Ti-Cr-rich oxides, are measured (Supplementary Data S5A) and described in the following text:

Olivine

Olivine compositions of both low and high vesicular İcik maar scoriae are given in Supplementary Data S5A. They are predominantly unzoned, with rare zoning observed in some crystals (e.g., $Fo_{71-68-71}$; Supplementary Data S5A). The core compositions range between Fo_{63-73} and Fo_{71-75}, respectively ($Fo = 100 \times Mg/[Mg + Fe^{2+} + Mn + Ca]$), which are comparable to other compositionally similar rocks (e.g., Süphan volcano) (Supplementary Figures S5A and B). The olivine Fo contents of the alkaline (Ne-normative) basalts from the Eğrikuyu Monogenetic Field (EMF, SW of the CAVP; Reid et al., 2017; Uslular and Gençalioğlu-Kuşcu, 2019) are higher (Supplementary Figures S5A and B).

The Fe/Mn ratios in the core compositions of olivine range from 45.7 to 64.3 in İcik maar (Supplementary Figure S5A). Except for the presence of a few lower ratios in İcik maar, the Fe/Mn contents are identical to the Quaternary rocks of the Süphan volcano. This ratio increases with increasing Fo content and forms a cluster around 75 mol % Fo for the İcik maar (Supplementary Figure S5A). The Ca contents in the core compositions of olivine are in the range of 1,000–2,000 ppm, which are similar to the compositionally equivalent Süphan volcanics (Supplementary Figure S5B).

Plagioclase

The plagioclase compositions of İcik maar scoriae are given in Supplementary Data S5B. The anorthite (An) contents of plagioclase cores in the İcik maar scoria range from 40 to 57 mol % (Supplementary Figure S5C and Supplementary Data S5B) with albite (Ab) and orthoclase (Or) compositions of Ab_{41-56} and Or_{2-4}, respectively (Supplementary Figure S5C and Supplementary Data S5B). These cores plot in the labradorite and andesine fields in the ternary feldspar diagram, while plagioclase from other mafic rocks around central Anatolia (i.e., EMF basalts) are mainly labradorites, with a small overlap in the bytownite field (Supplementary Figure S5C). As a compositional equivalent of İcik maar, the mugearitic Süphan volcanics have similar compositions ranging from labradorite to andesine (An_{30-55} and Ab_{43-65}; Supplementary Figure S5C).

Other mineral phases

The few orthopyroxene crystals, which were measured for İcik maar, were enstatitic in composition (En_{62-72}; Supplementary Data S5C), comparable to the pyroxene measured in the evolved volcanics across the CAVP (Aydar et al., 1995; Aydin, 2008; Köprübaşı et al., 2014; Doğan-Külahçı et al., 2018). Some of the measured accessory phases were Fe-Ti-Cr-rich oxides (Supplementary Data S5D).

Trace elements

The trace element compositions of studied maars are given in Supplementary Data S3. The contents of Cr, Sc, and Ni in the İcik maar scoriae change from 7 to 21 ppm, 18–20 ppm, and 10–60 ppm, respectively. Looking at all the mafic volcanic products around the Acıgöl caldera, we observe a positive correlation between these trace element concentrations and the MgO contents (considered as a differentiation index; Supplementary Figures S6A–C). The İcik maar scoriae are plotted on the low concentration end of these trace elements compared to the other mafics, but they generally have elevated trace element concentrations compared to felsic maars (Supplementary Figures S6D–F), except for the higher Rb contents of felsic maars (233–261 ppm; Supplementary Data S3). In addition, the İcik maar scoriae have comparable trace element concentrations with the older eastern domes in the Acıgöl caldera (Supplementary Figures S6D–F). The felsic maars and adjacent lava domes have positive trends for Sr/Nb vs Ba/Nb-Zr/Nb-La/Nb.

All the studied maars display light rare-earth element (LREE) enrichment with a relatively flat heavy REE in the

chondrite-normalized (McDonough and Sun, 1995) REE diagrams (Figures 12A and B). There is a significant Eu-anomaly in the felsic maars, which is absent in the İcik maar scoriae (Figures 12A and B). Here, the felsic volcanics including maars and adjacent lava domes have identical REE patterns (La/Lu_N = 2.2–3.2), whereas the İcik maar scoriae are slightly enriched especially in LREEs (La/Lu_N = 5.8–6.5).

The mid-ocean ridge basalts (MORB)- and primitive mantle (PM)-normalized (McDonough and Sun, 1995) multi-element patterns of the studied maars (felsic maars and İcik) are similar to trends typically formed by subduction-related volcanic rock, with the depletion of Nb, Ta, Ti, and P (Figures 12C and D). The felsic maars are enriched in large-ion lithophile elements (LILE) compared to the N-MORB, whereas they have identical high-field strength element (HFSE) contents (Figure 12C) and are significantly depleted in Sr, Ba, and Ti. The İcik maar scoriae have higher contents of both LILE and HFSE compared to the PM composition with slight depletions in Sr and Ba (Figure 12D).

Discussion

Maar facies architecture: Implications for eruption dynamics

The tephra (or ejecta) ring deposits of maars are one of the key proxies for the understanding of their complex evolutionary mechanisms (Németh et al., 2008; Lefebvre et al., 2013; Graettinger and Valentine, 2017; Lorenz et al., 2017; Ort et al., 2018). The recent advances in the maar literature (Graettinger, et al., 2015; Valentine et al., 2017) have coined the term "scaled depth (SD)," which is the ratio between the depth of explosion and the releasing energy (Goto et al., 2001). The position of the explosion locus (i.e., molten fuel coolant interaction "MFCI" between uprising magma and groundwater; Zimanowski et al., 1997) with respect to the optimum SD (OSD; ~0.004 $m/J^{1/3}$; Goto et al., 2001) during the maar formation can be tracked *via* the variations observed in the exposed maar stratigraphy (Graettinger et al., 2015). The finer surge deposits without or with limited block-sized materials represent the explosions deeper than the OSD, whereas the intercalation of fine surges and ballistically emplaced deposits indicates the near-optimal scaled depth explosions (Graettinger et al., 2015). In shallower explosions, the resultant deposits consist predominantly of block-rich ballistic curtain deposits (Graettinger et al., 2015).

The studied maar deposits serve as a helpful tool to investigate the possible changes in the explosion depths to the OSD (Figure 13). Here, it is important to note that the interpretation regarding the relation between the ejecta ring and scaled depth is limited to the exposed maar (except for Kalecitepe) deposits (at least 2/3 of the whole deposits). We have described six maar lithofacies consisting mainly of the ballistic curtain (TBm_1, TBm_2, and TBm_3) and dilute surge (AT_1 and AT_2) deposits (Figure 5; Table 1). The lower parts of the felsic maar stratigraphies (İnallı, Acıgöl, and Korudağ) are mainly occupied by TBm_1 facies that probably represent the widening stage of the maar craters with the dry phreatomagmatic (or volatile-driven) explosions at near or slightly shallower depths compared to the OSD (denoted by 1 in Figure 13). The following stratigraphy in most felsic maars consists predominantly of base surge deposits implying near or slightly deeper explosion depths concerning the OSD (number 2 in Figure 13). The only exception here is the Acıgöl maar, which has an alternation of the ballistic curtain (TBm_3) and surge (AT_1) deposits through the upper units, possibly due to multiple explosions of coalescent craters (Figure 3C, Figure 5, and Figure 13). The uppermost unit in the felsic maar (TBm_2) represents the shallowest explosions (number 3 in Figure 13) overlaid by either dome extrusions (in the case of Acıgöl and Korudağ maars) and/or meter-sized lithic blocks (Acıgöl maar; Figures 3D and F). The measured densities in felsic maars from this study decrease through the uppermost parts of the stratigraphy (Figure 5). This agrees with the presence of juvenile-rich TBm_2 facies, including more vesicular clasts formed predominantly by magmatic (or volatile-driven) explosions. As the İcik maar has been synchronously formed with the adjacent scoria cone (i.e., intercalated deposits; Figure 4B and Figure 5), it is difficult to make interpretations related to the OSD. However, it can be noted that the explosions are likely to have occurred near-surface or at shallower depths (per OSD), as revealed by the presence of ballistically emplaced lithic blocks found in the ash- to lapilli-rich base surges throughout the stratigraphy (Figure 13).

In addition to the role of SD and other properties (e.g., pre-existing topography, basement rocks; Lorenz, 2003; Auer et al., 2007; Carrasco-Núñez et al., 2007; Graettinger et al., 2015; Valentine et al., 2017), the depositional and compositional variations within the individual maars and among the felsic and mafic counterparts are also crucial, but their report is missing in the maar literature. Ross et al. (2017) revealed some of the similarities between felsic and mafic maars by adapting the former ones from their sister tuff rings. Together with a few similarities between these two end-members (e.g., comparable crater shapes and tephra ring thickness), Ross et al. (2017) also asserted a transition from phreatomagmatic to magmatic activity in the formation of felsic maars. This is also notable in the depositional characteristics of the studied felsic maars (Figure 5). Although significant portions of the stratigraphy are dominated by the phreatomagmatic deposits (i.e., AT_1 facies; Figure 5), the last ~50 cm of felsic maar deposits is typically occupied by juvenile-rich facies (TBm_2 and LT_1). Similar facies have been observed in the tuff ring deposits (e.g., Tepexitl, Mexico; Austin-Erickson et al., 2011). Here, we suggest that they may represent the initial phase of the dome/plug explosions, which is also supported by the extensive lava

dome formations within or near the maar craters in the study area. Another important distinction among the studied maars is the different percentages of juvenile contents. The overall juvenile content of the felsic maars is significantly higher (~30%) than the mugearitic İcik maar (Figure 6). This is in line with the higher amounts of juveniles obtained in the felsic tuff rings that can be evaluated as the sisters of felsic maars (Sheridan and Updike, 1975; Austin-Erickson et al., 2011; Ross et al., 2017). However, felsic maars have, in general, not been studied enough to convincingly state that they commonly have a higher amount of juveniles.

The lack of accretionary lapilli in the studied maars and the limited soft-sediment deformation arguably mean a low water/magma ratio in their formations. This might also appertain to the changes in the eruption styles (phreatomagmatic vs magmatic) during the maar formation. However, Valentine et al. (2017) propounded that these changes are mostly controlled by the magma flux and the hydrogeological heterogeneities of the diatremes. Similarly, the formation of accretionary lapilli-free deposits may rather be linked to the eruption dynamics and the emplacement conditions of the pyroclastic density currents rather than the low water/magma ratios (Brown et al., 2010, 2012; Zimmer et al., 2010). For example, the abundance of TBm facies among the studied maars can be interpreted as the higher mass and thermal flux during their formations (Brown et al., 2010). Such eruptional conditions also preclude the formation of accretionary lapilli in surges as they probably become more dilute with inadequate moisture (Brown et al., 2010). In addition, the emplacement conditions of the studied surges were possibly too hot for the condensation of water (Sohn and Chough, 1989; Zimmer et al., 2010).

Emplacement of monogenetic volcanoes in the Acıgöl caldera

The mafic monogenetic cluster consisting of coalescent maar and scoria cone

After a period of quiescence in the volcanism within the Acıgöl caldera (~100 ka) following the ignimbrite-forming eruptions (Druitt et al., 1995; Schmitt et al., 2011), the monogenetic activity (32 ± 3 ka; Türkecan et al., 2004) took place in the eastern part of the caldera along an N-S oriented intrusion (~1.5 km length) where the İcik maar with two nested craters and an adjacent scoria cone was formed (Figure 1C and Figure 2). The volcanic activity was probably initiated by the fissure-type eruptions that formed blocky lava flows found in the northern parts of the depression (Figure 4D and Figure 13). The latter phase with a possible time gap is represented by the syn-eruptive activity of both coalescent maar craters and a scoria cone, which is revealed by the intercalated deposits in the maar stratigraphy (Figure 5). The activity ends with the formation of scoria-cone-related lava flows that overlay the maar deposits (Figure 5 and Figure 13). Here, it can be argued that the variation in magma flux within a few hundred-meter distances, probably due to the localized water bodies in the fractured aquifers, directly determines the eruption styles and the resultant monogenetic edifices (Amin and Valentine, 2017). In addition, we claim that there is one feeder dike system, which is possibly rejuvenated by the post maar and scoria cone formation (Figure 13). Lastly, the age of the maar can be considered the same as the scoria cone (32 ± 3 ka; Türkecan et al., 2004) due to their synchronous activity as observed in the deposits. However, any future age data obtained directly from the proximal maar deposits would certainly better clarify the eruption sequences in the İcik maar.

The felsic monogenetic cluster including maars and lava domes

The relatively younger activity (~25–20 ka; Schmitt et al., 2011) responsible for the NW-SE-oriented clustering of rhyolitic maars and adjacent lava domes took place along a ~10 km-long intrusion in the western part of the Acıgöl caldera (Figure 1C). The elongations of the maar rims (especially İnallı and Kalecitepe; Figure 1C) follow an NW-SE direction (i.e., N102°-113°), which is both parallel to the possible dike system and the main trend of the Tuzgolü Fault Zone (Çemen et al., 1999). As for the initiation of phreatomagmatic eruptions along this cluster, the uprising magma fed by several dikes possibly reached the fractured aquifers (i.e., andesitic lavas and crystalline rocks) at relatively shallow depths and resulted in the formation of maars (Figure 13). This is supported by the observed large lithics (up a few meters) and the described maar lithofacies (Figure 3 and Figure 5). Through the end of the stratigraphy at felsic maars (i.e., TBm_2 facies), the role of phreatomagmatism has been significantly decreased, possibly due to the increase in the magma flux that results in the formation of syn- or post-emplacement of lava domes (Figure 13).

The lateral movement of the rising magma is rather evident, as in the case of the Acıgöl maar and the adjacent lava dome, possibly due to the topographic unloading (Acocella, 2021) during the maar formation (Figure 2; Figure 13). Here, we suggest the presence of at least four coalescent craters, one of which is almost completely deformed by the subsequent lava dome emplacement (Figure 1C, Figure 2, and Figure 13). Reliable ages obtained directly from maar juveniles are only available for the northwestern crater of the Acıgöl maar (20.3 ± 0.9 ka; Schmitt et al., 2011) that somehow postdates the adjacent Güneydağ lava dome extrusion (23.8 ± 2.1 ka; Schmitt et al., 2011). This leads some of the previous studies in the region to suggest that the maars are formed after the lava domes (Mouralis et al., 2019). However, our field-based observations are not concordant with these ages, and we argue that there is an age discrepancy most probably due to the close (even successive) time interval among the maar and

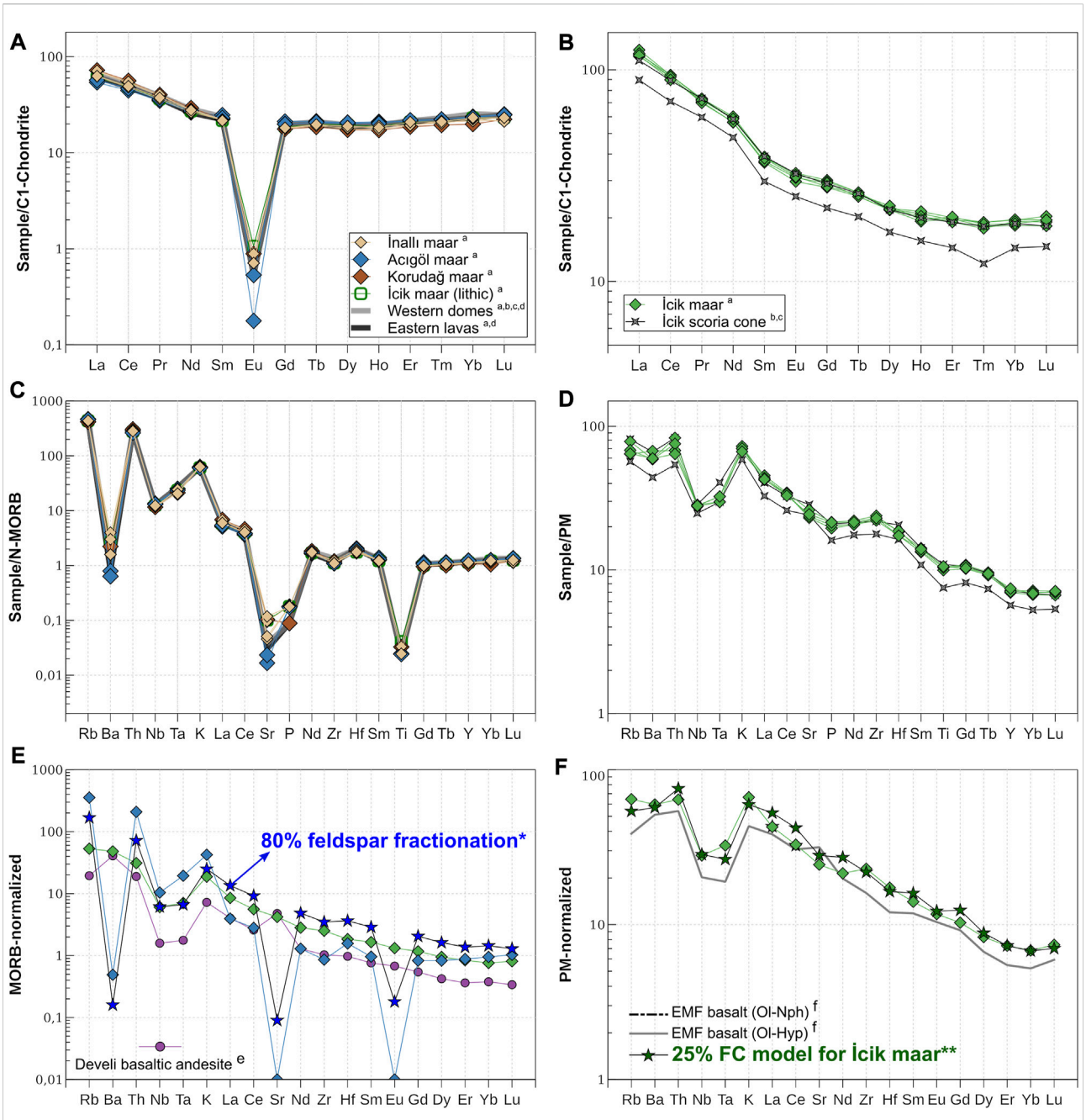

FIGURE 12
Chondrite-normalized REE diagrams of **(A)** the studied felsic maars together with one lithic from İcik maar and the compiled lava domes within the Acıgöl caldera (a this study; b Türkecan et al., 2004; c Aydar et al., 2011; d Siebel et al., 2011) and **(B)** İcik maar and adjacent scoria cone. The multi-element patterns of **(C)** N-MORB-normalized felsic maar compositions and **(D)** PM-normalized İcik volcanics. **(E)** The AFC model for the studied felsic maars (e.g., Acıgöl). *80% FC (5% Ol and Cpx, 65% Pl, and 25% Snd) of evolved volcanics in the CAVP (e.g., Develi basaltic andesite, Aluç et al., 2020[e]). **(F)** The FC model for the İcik maar. ** 25% FC (0.15% Ol, 0.35% Cpx, 0.15% Opx, 0.37% Pl, and 0.03% Snd) of Ol-Hyp normative EMF basalt (Uslular and Gençalioğlu-Kuşcu, 2019[f]).

lava dome formations. Therefore, the relatively younger age should not imply that the volcanic activity in this cluster lasted with the maar formation, which is not supported by our recent findings (e.g., lack of post-deformational imprints in the observed deposits and uplifting of the adjacent maar craters due to the lava dome extrusion). However, our reconstruction still needs some further investigations (e.g., dating and geophysics) to better constrain the evolutionary model.

Magma source characteristics

The studied maars in the Acıgöl caldera (~20–32 ka; Türkecan et al., 2004; Schmitt et al., 2011) and the Holocene lava domes in the flanks of Erciyes stratovolcano (~9–10 ka; e.g., Friedrichs et al., 2021) represent the youngest monogenetic activity in the CAVP. Both felsic and mafic maars in the Acıgöl caldera carry a typical subduction inheritance in their trace element compositions (depletion in Nb, Ta, Ti, and P), which is the general characteristic of all volcanics in the CAVP, including the most alkaline basalts (Reid et al., 2017; Uslular and Gençalioğlu-Kuşcu, 2019). The exception here is the higher alkalinity (up to ~7 wt% Na_2O+ K_2O) of maars and some of the other volcanics in and around the Acıgöl caldera compared to other CAVP volcanics (Figure 10A). We investigate the possible underlying mechanisms explaining this difference and the evolution of the volcanics, with the assimilation and fractional crystallization (AFC) models using several possible source compositions (Figures 12E and F) (see Supplementary Material for details).

Our models show that the AFC is the dominant mechanism in the formation of magma feeding the studied maars. The mugearitic İcik maar and the adjacent volcanics can be generated by fractional crystallization (10–15% olivine, 30–35% clinopyroxene, 5–10% orthopyroxene, 30–35% plagioclase, and 0.3–0.5% sanidine) of the Ol-Hyp normative EMF transitional basalt, which is formed by heterogeneous mantle source (Uslular and Gençalioğlu-Kuşcu, 2019) (Figure 12E and Supplementary Material). The possible differentiation trends in the whole-rock compositions of the İcik scoriae also support the fractional crystallization model (Figure 11). The negative trends of MgO and CaO vs SiO_2 contents, together with the increase in Sc, Ni, and Cr with the increase in MgO, are the possible indications for olivine, pyroxene, and plagioclase fractionation (Figures 11 and 12). Olivine fractionation is also evident in the slightly negative trends between Fo (for >70%) and Ca (ppm) (Supplementary Figure S5A). This relation becomes more scattered in the lower Fo contents, where the fractionation is dominated by other phases (pyroxene and plagioclase).

The felsic maars have also various imprints of the AFC in their whole-rock compositions (Figures 11 and 12 and Supplementary Figure S6). The aphyric rhyolites can be formed through 70–80% crystal fractionation of the calc-alkaline Develi (NE of CAVP) basaltic andesite (~6 Ma; Aluç et al., 2020), which is suggested to represent some crustal contamination (~10–20%) by the basement granites (e.g., Terlemez granitoids; Yalınız et al., 1999) (Figure 12E). In our crystallization model, the modal proportions of feldspars are higher (60–70%) than the mafic phases (5–10%). Although generating rhyolites through crystal fractionation of less evolved magmas is a rather common mechanism (Streck and Grunder, 2008), several alternative models also exist, for example, the long-lived crystallization or intermittent melting in a closed system, and the presence of crustal melts (Simon and Reid, 2005; Streck and Grunder, 2008; Loewen and Bindeman, 2015). Hence, the younger rhyolite group (including the maars) might have been formed by fractionation of a magma source that also formed the older eastern domes within a long-lived closed system. The significant temporal decrease in feldspar-compatible major (CaO and Al_2O_3) and trace (Sr, La, and Ba) elements, together with the decrease in Zr, can be due to the fractionation of feldspars with minor accessory phases (e.g., zircon and chevkinite; Loewen and Bindeman, 2015) (Supplementary Figure S6). However, the different zircon oxygen isotope contents of younger and eastern domes (6.2 ± 0.2‰ and 5.7 ± 0.2‰, respectively) somehow preclude the possible presence of a long-lived magma chamber beneath the Acıgöl caldera (Schmitt et al., 2011; Siebel et al., 2011). Instead, these temporarily distinct rhyolitic activities were mutually exclusive with the episodic inputs of parental mafic magma ponded at lower crustal levels (Siebel et al., 2011; and this study). This is also supported by the spatial distribution of the vents in the region (i.e., non-clustered; Uslular et al., 2021).

The Acıgöl caldera overlies a crystalline basement consisting of granites, ophiolites, and metamorphosed rocks (Floyd et al., 1998). The heterogeneous mantle-derived magma source, which is mostly responsible for widespread Quaternary volcanism in the CAVP (Gençalioğlu-Kuşcu and Geneli, 2010; Reid et al., 2017; Di Giuseppe et al., 2018; Uslular and Gençalioğlu-Kuşcu, 2019), is probably trapped at the crustal levels with low-density barriers in the Acıgöl caldera (Loewen and Bindeman, 2015) and can reach the surface *via* local faults if available (Derinkuyu, Toprak, 1998). This possibly favors the assimilation and fractional crystallization processes, and results in the formation of less voluminous basaltic volcanism in the region. In addition, the emplacement of studied monogenetic complexes along the probable parallel dike intrusions is also in line with the significant role of tectonism in the widespread Quaternary volcanism in the CAVP (Toprak and Göncüoğlu, 1993; Toprak, 1998; Higgins et al., 2015; Uslular et al., 2021). As for the recent discussions on the lithology of mantle source in the CAVP suggesting a pyroxenite inheritance (Gall et al., 2021; Gençoğlu-Korkmaz et al., 2021), we could not provide any contribution with our findings on the mafic İcik maar due to its slightly evolved composition. However, it is evident from the olivine compositions of EMF alkali basalts, which are close to both pyroxenite- and peridotite-bearing mantle sources (Herzberg, 2011; Søager et al., 2015) (Supplementary Figure S5A). Further studies especially on the mantle xenoliths and isotope compositions of mafics across the CAVP, including the Acıgöl region, are required for a better constraint of the mantle source. Lastly, the low-velocity anomalies, the shallow Curie depths (9–11 km), and the widespread geothermal activity in and around the Acıgöl caldera (Kıyak et al., 2015; Abgarmi et al., 2017; Bilim et al., 2017) merit further

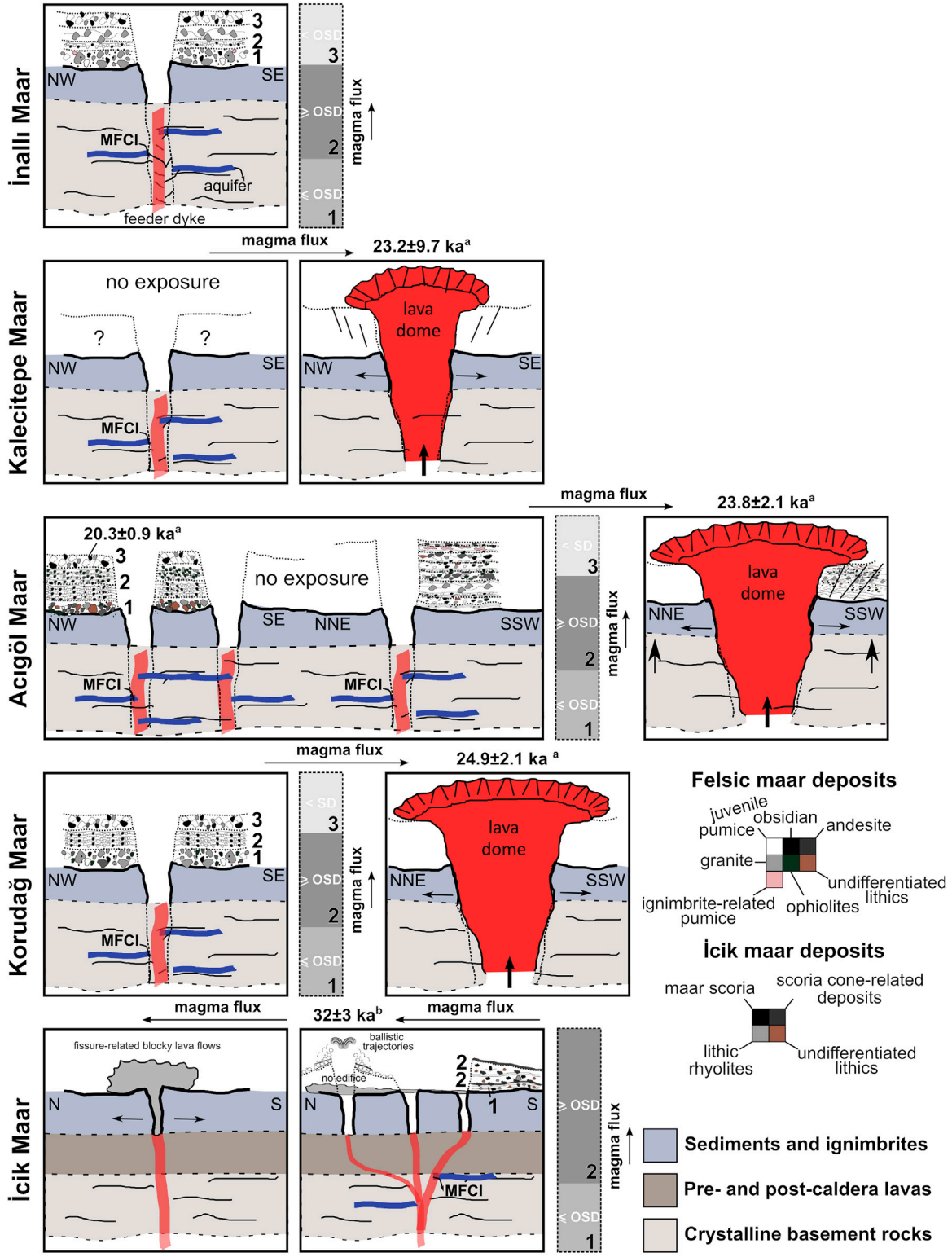

FIGURE 13
Proposed evolutionary model for the maars and the adjacent monogenetics in the Acıgöl caldera. The figures are not to scale. [a] Schmitt et al. (2011); [b] Türkecan et al. (2004).

volcanic hazard assessment of the region to determine the likelihood and style of the future volcanic activity (Newhall et al., 2018).

Conclusion

Our detailed field observations and laboratory analysis, together with the physical volcanology and geochemical analyses of mafic and felsic maars within the Acıgöl caldera led us to the following conclusion:

- The scaled depth, magma flux, and hydrogeological heterogeneities in the diatremes are the leading mechanisms that mostly shape the depositional characteristics of the maars. The vertical and horizontal movement of the eruption locus and the presence of successive (felsic maars and lava domes) or coeval (İcik maar and scoria cone) phreatomagmatic and magmatic eruptions during the formation of studied monogenetic complexes are the most significant findings in this study. The transition in the eruptive styles, evident at both outcrop- and juvenile clast-scale, is also notable in the formation of an individual felsic maar similar to the felsic tuff rings.
- The magmatic and phreatomagmatic explosions in edifice- and field-scale monogenetic activity can be generated both synchronously and successively. The volcanic activity in the İcik mafic monogenetic complex was possibly initiated with a fissure-type eruption widening the smaller N-S trending intrusion and then continuing with the synchronous formation of coalescent maars and a scoria cone. As for the felsic monogenetic group outcropped along the longer NW-SE trending intrusion in the western part of the Acıgöl caldera, the monogenetic activity possibly started with the phreatomagmatic eruptions that form the maars (İnallı, Kalecitepe, Acıgöl, and Korudağ). Through the end of this maar-forming stage, the monogenetic activity became magmatic (or dry phreatomagmatic), evident by the presence of juvenile-rich blocky deposits in the maar stratigraphy. This was followed by the emplacement of rhyolitic lava domes that mostly deformed the maar rims and ejecta deposits. This evolutionary model for the felsic monogenetic group is not congruent with the available age of Acıgöl maar, which is slightly younger than the adjacent lava dome. Therefore, here, we state that there is a need for more age data obtained directly from the maar juveniles in the region.
- The multi-element patterns of studied rhyolitic and mugearitic maars are almost identical in terms of depletions in Nb, Ta, P, and Ti as a typical indication for the subduction-inheritance in their formations similar to all Quaternary volcanics in the CAVP. The mugearitic İcik maar and adjacent volcanics can be formed by the fractional crystallization (partly with the assimilation) processes of the slightly evolved version of a parental magma (i.e., identical to Ol-Hyp normative EMF basalt). However, the extensive (70–80%) feldspar fractionation of any evolved composition in the CAVP with minor crustal contamination *via* basement granites is considered a suitable process for the evolution of felsic maars and adjacent lava domes.

In conclusion, our recent findings on both felsic and mafic maars indicate the complex evolutionary processes of maars formed by various explosions at different depths below a few hundred meters of the craters rather than the progressive deepening of the explosion locus. Some of the distinct features of felsic maars (e.g., higher juvenile content and less evidence of sedimentary structure) revealed in this study also contribute to the understanding of the lesser known part of maar volcanism compared to their more common mafic counterparts, even if any generalization can be misleading due to the dynamic behavior of the maars (e.g., changes in hydrogeological conditions, basement lithology, and pre-existing topography). Additionally, our main future perspective for the youngest monogenetic activity in the Acıgöl caldera is the need for geochronology and geophysical studies to better constrain its evolutionary processes.

Data availability statement

The datasets presented in this study can be found in online repositories. The names of the repository/repositories and accession number(s) can be found in the article/ Supplementary Material.

Author contributions

GU: conceptualization, formal analysis, and writing—original draft; GG: review—editing and supervision; FB: mineral chemistry, review—editing, and supervision; JR: review—editing and supervision; ML: review—editing and supervision; OH: mineral chemistry and review—editing; LC: review—editing and supervision.

Funding

The Scientific and Technical Research Council of Turkey (TÜBİTAK) and the Scientific Research Project Office of Muğla Sıtkı Koçman University (MSKU, Turkey) financially supported

this study with grant numbers 118Y360 and 19/077/09/2, respectively. For the period of stay in Geneva, GU was granted a scholarship given by the Council of Higher Education in Turkey (YUDAB 2019), and housing aid was provided by the University of Geneva (UNIGE, Switzerland). This study is a part of Cotutelle PhD thesis by GU carried out between Muğla Sıtkı Koçman University (MSKU, Turkey) and the University of Geneva (UNIGE, Switzerland). Open access funding was provided by the University of Geneva.

Acknowledgments

GU is grateful to Rana Salihoğlu, Mustafa Erde Bilir, and Jean-Marie Boccard for the preparation of thin sections. Dr Tuba Baygar is also thanked for her help during the SEM analyses. The authors especially thank Dr İnan Ulusoy, Dr Murat Gül, and the Volcano-Tectonic laboratory members at UNIGE (Dr Marine Collignon, Stefano Mannini, and Elisabetta Panza) for their fruitful discussions and recommendations. The authors deeply appreciate the valuable and constructive comments of the chief editor Valerio Acocella, the guest editor AG, and two reviewers.

Conflict of interest

The authors declare that the research was conducted in the absence of any commercial or financial relationships that could be construed as a potential conflict of interest.

Publisher's note

Supplementary material

The Supplementary Material for this article can be found online at: https://www.frontiersin.org/articles/10.3389/feart.2022.909951/full#supplementary-material

References

Abgarmi, B., Delph, J. R., Özacar, A. A., Beck, S. L., Zandt, G., Sandvol, E., et al. (2017). Structure of the crust and African slab beneath the central Anatolian plateau from receiver functions: New insights on isostatic compensation and slab dynamics. *Geosphere* 13, 1774–1787. doi:10.1130/ges01509.1

Acocella, V. (2021). *Volcano-tectonic processes*. Switzerland: Springer Nature, 552.

Aluç, A., Kuşcu, İ., Peytcheva, I., Cihan, M., and von Quadt, A. (2020). The late Miocene Öksüt high sulfidation epithermal Au-Cu deposit, Central Anatolia, Turkey: Geology, geochronology, and geochemistry. *Ore Geol. Rev.* 126, 103795. doi:10.1016/j.oregeorev.2020.103795

Amin, J., and Valentine, G. A. (2017). Compound maar crater and co-eruptive scoria cone in the Lunar Crater Volcanic Field (Nevada, USA). *J. Volcanol. Geotherm. Res.* 339, 41–51. doi:10.1016/j.jvolgeores.2017.05.002

Atıcı, G., Schmitt, A. K., Friedrichs, B., Sparks, S., Danisık, M., Yurteri, E., et al. (2019). Ages and glass compositions for paired large-volume eruptions from the Acigol volcanic complex, Cappadocia (Turkey). *Med. Geosc. Rev.* 1, 167–178. doi:10.1007/s42990-019-00013-5

Auer, A., Martin, U., and Nemeth, K. (2007). The Fekete-hegy (Balaton Highland Hungary) "soft-substrate" and "hard-substrate" maar volcanoes in an aligned volcanic complex–Implications for vent geometry, subsurface stratigraphy and the palaeoenvironmental setting. *J. Volcanol. Geotherm. Res.* 159, 225–245. doi:10.1016/j.jvolgeores.2006.06.008

Austin-Erickson, A., Ort, M. H., and Carrasco-Nunez, G. (2011). Rhyolitic phreatomagmatism explored: Tepexitl tuff ring (eastern Mexican volcanic belt). *J. Volcanol. Geotherm. Res.* 201, 325–341. doi:10.1016/j.jvolgeores.2010.09.007

Aydar, E., Çubukçu, E., Ulusoy, İ., Şen, E., Yürür, M. T., Ekmekçi, M., et al. (2011). *Nevşehir kalderasının volkanolojik-petrolojik evriminin ve tektonizma-volkanizma ilişkisinin zaman ve mekan içinde incelenmesi*.Ankara: Tech. rep., TUBITAK Project No.108Y063.

Aydar, E., Gourgaud, A., Deniel, C., Lyberis, N., and Gündoğdu, N. (1995). Le volcanisme quaternaire d'Anatolie centrale (Turquie): Association de magmatismes calco-alcalin et alcalin en domaine de convergence. *Can. J. Earth Sci.* 32 (7), 1058–1069. doi:10.1139/e95-087

Aydar, E., Schmitt, A. K., Çubukçu, H. E., Akin, L., Ersoy, O., Sen, E., et al. (2012). Correlation of ignimbrites in the central Anatolian volcanic province using zircon and plagioclase ages and zircon compositions. *J. Volcanol. Geotherm. Res.* 213, 83–97. doi:10.1016/j.jvolgeores.2011.11.005

Aydin, F. (2008). Contrasting complexities in the evolution of calc-alkaline and alkaline melts of the Nigde volcanic rocks, Turkey: Textural, mineral chemical and geochemical evidence. *Eur. J. Mineral.* 20 (1), 101–118. doi:10.1127/0935-1221/2008/0020-1784

Bilim, F., Kosaroglu, S., Aydemir, A., and Buyuksarac, A. (2017). Thermal investigation in the Cappadocia region, Central Anatolia-Turkey, analyzing Curie point depth, geothermal gradient, and heat-flow maps from the aeromagnetic data. *Pure Appl. Geophys.* 174 (12), 4445–4458. doi:10.1007/s00024-017-1666-z

Blott, S. J., and Pye, K. (2001). GRADISTAT: A grain size distribution and statistics package for the analysis of unconsolidated sediments. *Earth Surf. Process. Landf.* 26 (11), 1237–1248. doi:10.1002/esp.261

Borrero, C., Murcia, H., Agustin-Flores, J., Arboleda, M. T., and Giraldo, A. M. (2017). Pyroclastic deposits of San Diego maar, central Colombia: An example of a silicic magma-related monogenetic eruption in a hard substrate. *Geol. Soc. Lond. Spec. Publ.* 446 (1), 361–374. doi:10.1144/SP446.10

Branney, M. J., and Kokelaar, P. (2002). *Pyroclastic density currents and the sedimentation of ignimbrites*. London: Geological Society Memoir No. 27.

Brown, R. J., Bonadonna, C., and Durant, A. J. (2012). A review of volcanic ash aggregation. *Phys. Chem. Earth, Parts A/B/C* 45, 65–78. doi:10.1016/j.pce.2011.11.001

Brown, R. J., Branney, M. J., Maher, C., and Davila-Harris, P. (2010). Origin of accretionary lapilli within ground-hugging density currents: Evidence from pyroclastic couplets on Tenerife. *Geol. Soc. Am. Bull.* 122 (1–2), 305–320. doi:10.1130/B26449.1

Cañón-Tapia, E. (2016). Reappraisal of the significance of volcanic fields. *J. Volcanol. Geotherm. Res.* 310, 26–38. doi:10.1016/j.jvolgeores.2015.11.010

Carrasco-Núñez, G., Ort, M. H., and Romero, C. (2007). Evolution and hydrological conditions of a maar volcano (Atexcac crater, Eastern Mexico). *J. Volcanol. Geotherm. Res.* 159 (1–3), 179–197. doi:10.1016/j.jvolgeores.2006.07.001

Carrasco-Núñez, G., and Riggs, N. R. (2008). Polygenetic nature of a rhyolitic dome and implications for hazard assessment: Cerro Pizarro volcano, Mexico. *J. Volcanol. Geotherm. Res.* 171 (3–4), 307–315. doi:10.1016/j.jvolgeores.2007.12.002

Çemen, İ., Göncüoğlu, M. C., and Dirik, K. (1999). Structural evolution of the tuzgölü basin in central Anatolia, Turkey. *J. Geol.* 107, 693–706. doi:10.1086/314379

Chako Tchamabé, B., Carrasco-Núñez, G., Miggins, D. P., and Németh, K. (2020). Late pleistocene to Holocene activity of alchichica maar volcano, eastern trans-Mexican volcanic belt. *J. S. Am. Earth Sci.* 97, 102404. doi:10.1016/j.jsames.2019.102404

Chako Tchamabé, B., Kereszturi, G., Németh, K., and Carrasco-Núñez, G. (2016). "How polygenetic are monogenetic volcanoes: Case studies of some complex maar-diatreme volcanoes," in *Updates in volcanology—from volcano modelling to Volcano geology*. Editor K. Nemeth (Rijeka, Croatia: InTech). doi:10.5772/63486

Congedo, L. (2021). Semi-automatic classification plugin: A Python tool for the download and processing of remote sensing images in QGIS. *J. Open Source Softw.* 6, 3172. doi:10.21105/joss.03172

De León-Barragán, L., Carrasco-Núñez, G., and Ort, M. H. (2020). Stratigraphy and evolution of the Holocene aljojuca maar volcano (Serdán-Oriental basin, eastern trans-Mexican volcanic belt), and implications for hazard assessment. *J. Volcanol. Geotherm. Res.* 392, 106789. doi:10.1016/j.jvolgeores.2020.106789

Di Giuseppe, P., Agostini, S., Manetti, P., Savaşçın, M. Y., and Conticelli, S. (2018). Sub-lithospheric origin of Na-alkaline and calc-alkaline magmas in a post-collisional tectonic regime: Sr-Nd-Pb isotopes in recent monogenetic volcanism of cappadocia, central Turkey. *Lithos* 316, 304–322. doi:10.1016/j.lithos.2018.07.018

Di Traglia, F., Cimarelli, C., de Rita, D., and Gimeno Torrente, D. (2009). Changing eruptive styles in basaltic explosive volcanism: Examples from Croscat complex scoria cone, Garrotxa Volcanic Field (NE Iberian Peninsula). *J. Volcanol. Geotherm. Res.* 180 (2–4), 89–109. doi:10.1016/j.jvolgeores.2008.10.020

Doğan-Külahçı, G. D., Temel, A., Gourgaud, A., Varol, E., Guillou, H., and Deniel, C. (2018). Contemporaneous alkaline and calc-alkaline series in Central Anatolia (Turkey): Spatio-temporal evolution of a post-collisional Quaternary basaltic volcanism. *J. Volcanol. Geotherm. Res.* 356, 56–74. doi:10.1016/j.jvolgeores.2018.02.012

Druitt, T. H., Brenchley, P. J., Gökten, Y. E., and Francaviglia, V. (1995). Late quaternary rhyolitic eruptions from the acigöl complex, central Turkey. *J. Geol. Soc. Lond.* 152 (4), 655–667. doi:10.1144/gsjgs.152.4.0655

Emre, O., Duman, T., Özalp, S., Elmacı, H., and Olgun, Ş. (2011). *1:250,000 scale Active fault map series of Turkey, kayseri (NJ 36-8) quadrangle*. Ankara, Turkey: General Directorate of Mineral Research and Exploration. Serial Number: 32. Tech. rep.

Ersoy, O., Aydar, E., Şen, E., and Gourgaud, A. (2019). Contrasting fragmentation and transportation dynamics during the emplacement of Dikkartın rhyodacitic dome; Erciyes stratovolcano, central Turkey. *Med. Geosc. Rev.* 1 (2), 223–242. doi:10.1007/s42990-019-00014-4

Floyd, P., Yaliniz, M. K., and Göncüoglu, M. C. (1998). Geochemistry and petrogenesis of intrusive and extrusive ophiolitic plagiogranites, Central Anatolian Crystalline Complex, Turkey. *Lithos* 42 (3–4), 225–241. doi:10.1016/S0024-4937(97)00044-3

Friedrichs, B., Atıcı, G., Danisık, M., Yurteri, E., and Schmitt, A. K. (2021). Sequence modeling in zircon double-dating of early Holocene Mt. Erciyes domes (Central Anatolia). *Quat. Geochronol.* 61, 101129. doi:10.1016/j.quageo.2020.101129

Friedrichs, B., Schindlbeck-Belo, J. C., Danisık, M., Jenkins, S. F., Yurteri, E., Çobankaya, M., et al. (2020). New insights into source and dispersal of Mediterranean S1 tephra, an early Holocene marker horizon erupted at Mt. Erciyes (Turkey). *Quat. Sci. Rev.* 249, 106606. doi:10.1016/j.quascirev.2020.106606

Froger, J.-L., Lénat, J.-F., Chorowicz, J., Le Pennec, J.-L., Bourdier, J.-L., Köse, O., et al. (1998). Hidden calderas evidenced by multisource geophysical data; example of Cappadocian Calderas, Central Anatolia. *J. Volcanol. Geotherm. Res.* 85 (1–4), 99–128. doi:10.1016/S0377-0273(98)00052-3

Frost, B. R., and Frost, C. D. (2008). A geochemical classification for feldspathic igneous rocks. *J. Petrology* 49, 1955–1969. doi:10.1093/petrology/egn054

Gall, H., Furman, T., Hanan, B., Kürkçüoğlu, B., Sayıt, K., Yürür, T., et al. (2021). Post-delamination magmatism in south-Central Anatolia. *Lithos* 398, 106299. doi:10.1016/j.lithos.2021.106299

Genç, Y., and Yürür, M. T. (2010). Coeval extension and compression in Late Mesozoic–Recent thin-skinned extensional tectonics in Central Anatolia, Turkey. *J. Struct. Geol.* 32, 623–640. doi:10.1016/j.jsg.2010.03.011

Gençalioğlu Kuşcu, G., and Geneli, F. (2010). Review of post-collisional volcanism in the central anatolian volcanic province (Turkey), with special reference to the tepekoy volcanic complex. *Int. J. Earth Sci.* 99 (3), 593–621. doi:10.1007/s00531-008-0402-4

Gençalioğlu-Kuşcu, G., Atilla, C., Cas, R. A. F., and Kuşcu, İ. (2007). Base surge deposits, eruption history, and depositional processes of a wet phreatomagmatic volcano in Central Anatolia (Cora Maar). *J. Volcanol. Geotherm. Res.* 159 (1–3), 198–209. doi:10.1016/j.jvolgeores.2006.06.013

Gençalioğlu-Kuşcu, G. (2011). Geochemical characterization of a quaternary monogenetic volcano in Erciyes volcanic complex: Cora maar (central anatolian volcanic province, Turkey). *Int. J. Earth Sci.* 100 (8), 1967–1985. doi:10.1007/s00531-010-0620-4

Gençoğlu-Korkmaz, G., Hüseyin, K., and Kürşad, A. (2021). Classification and generation of the enclaves in Karapınar-Karacadağ volcanic rocks (Central Anatolia). *Turkish J. Geosciences* 2, 30–46.

Geshi, N., Németh, K., and Oikawa, T. (2011). Growth of phreatomagmatic explosion craters: A model inferred from suoana crater in miyakejima volcano, Japan. *J. Volcanol. Geotherm. Res.* 201 (1–4), 30–38. doi:10.1016/j.jvolgeores.2010.11.012

Gevrek, A. İ., and Kazancı, N. (2000). A Pleistocene, pyroclastic-poor maar from Central Anatolia, Turkey: Influence of a local fault on a phreatomagmatic eruption. *J. Volcanol. Geotherm. Res.* 95 (1–4), 309–317. doi:10.1016/S0377-0273(99)00121-3

Goto, A., Taniguchi, H., Yoshida, M., Ohba, T., and Oshima, H. (2001). Effects of explosion energy and depth to the formation of blast wave and crater: Field Explosion Experiment for the understanding of volcanic explosion. *Geophys. Res. Lett.* 28 (22), 4287–4290. doi:10.1029/2001GL013213

Graettinger, A. H. (2018). Trends in maar crater size and shape using the global Maar Volcano Location and Shape (MaarVLS) database. *J. Volcanol. Geotherm. Res.* 357, 1–13. doi:10.1016/j.jvolgeores.2018.04.002

Graettinger, A. H., and Valentine, G. A. (2017). Evidence for the relative depths and energies of phreatomagmatic explosions recorded in tephra rings. *Bull. Volcanol.* 79 (12), 88. doi:10.1007/s00445-017-1177-x

Graettinger, A. H., Valentine, G. A., Sonder, I., Ross, P.-S., and White, J. D. L. (2015). Facies distribution of ejecta in analog tephra rings from experiments with single and multiple subsurface explosions. *Bull. Volcanol.* 77 (8), 66. doi:10.1007/s00445-015-0951-x

Herzberg, C. (2011). Identification of source lithology in the Hawaiian and canary islands: Implications for origins. *J. Petrology* 52, 113–146. doi:10.1093/petrology/egq075

Higgins, M., Schoenbohm, L. M., Brocard, G., Kaymakçı, N., Gosse, J. C., and Cosca, M. A. (2015). New kinematic and geochronologic evidence for the Quaternary evolution of the Central Anatolian fault zone (CAFZ). *Tectonics* 34 (10), 2118–2141. doi:10.1002/2015tc003864

Higgins, O., Sheldrake, T., and Caricchi, L. (2021). Quantitative chemical mapping of plagioclase as a tool for the interpretation of volcanic stratigraphy: An example from Saint Kitts, Lesser Antilles. *Bull. Volcanol.* 83 (8), 51. doi:10.1007/s00445-021-01476-x

Hintz, A. R., and Valentine, G. A. (2012). Complex plumbing of monogenetic scoria cones: New insights from the lunar crater volcanic field (Nevada, USA). *J. Volcanol. Geotherm. Res.* 239 (240), 19–32. doi:10.1016/j.jvolgeores.2012.06.008

Houghton, B. F., and Schmincke, H.-U. (1986). Mixed deposits of simultaneous strombolian and phreatomagmatic volcanism: Rothenberg volcano, east Eifel volcanic field. *J. Volcanol. Geotherm. Res.* 30 (1–2), 117–130. doi:10.1016/0377-0273(86)90069-7

Ingram, R. L. (1954). Terminology for the thickness of stratification and parting units in sedimentary rocks. *Geol. Soc. Am. Bull.* 65 (9), 937. doi:10.1130/0016-7606(1954)65[937:TFTTOS]2.0.CO;2

Inman, D. L. (1952). Measures for describing the size distribution of sediments. *SEPM J. Sediment. Res.* 22. doi:10.1306/D42694DB-2B26-11D7-8648000102C1865D

Irvine, T. N., and Baragar, W. (1971). *A guide to the chemical classification of the common volcanic rocks*.

Jankovics, M. É., Harangi, S., Németh, K., Kiss, B., and Ntaflos, T. (2015). A complex magmatic system beneath the Kissomlyó monogenetic volcano (Western Pannonian Basin): Evidence from mineral textures, zoning and chemistry. *J. Volcanol. Geotherm. Res.* 301, 38–55. doi:10.1016/j.jvolgeores.2015.04.010

Kazancı, N., Gevrek, A., and Varol, B. (1995). Facies changes and high calorific peat formation in a quaternary maar lake, Central Anatolia, Turkey: The possible role of geothermal processes in a closed lacustrine basin. *Sediment. Geol.* 94 (3–4), 255–266. doi:10.1016/0037-0738(94)00092-9

Keller, J. (1974). Quaternary maar volcanism near karapinar in Central Anatolia. *Bull. Volcanol.* 38 (1), 378–396. doi:10.1007/BF02599413

Kereszturi, G., and Németh, K. (2016). Sedimentology, eruptive mechanism and facies architecture of basaltic scoria cones from the Auckland Volcanic Field (New Zealand). *J. Volcanol. Geotherm. Res.* 324, 41–56. doi:10.1016/j.jvolgeores.2016.05.012

Kıyak, A., Karavul, C., Gulen, L., Pekişen, E., and Kılıç, A. R. (2015). Assessment of geothermal energy potential by geophysical methods: Nevşehir Region, Central Anatolia. *J. Volcanol. Geotherm. Res.* 295, 55–64. doi:10.1016/j.jvolgeores.2015.03.002

Köprübaşı, N., Güçtekin, A., Çelebi, D., and Kirmaci, M. Z. (2014). Mineral chemical constraints on the petrogenesis of mafic and intermediate volcanic rocks from the Erciyes and Hasandağ volcanoes, Central Turkey. *Geochemistry* 74 (4), 585–600. doi:10.1016/j.chemer.2013.11.003

Kósik, S., Németh, K., Lexa, J., and Procter, J. N. (2019). Understanding the evolution of a small-volume silicic fissure eruption: Puketerata volcanic complex, taupo volcanic zone, New Zealand. *J. Volcanol. Geotherm. Res.* 383, 28–46. doi:10.1016/j.jvolgeores.2017.12.008

Lefebvre, N. S., White, J. D. L., and Kjarsgaard, B. A. (2013). Unbedded diatreme deposits reveal maar-diatreme-forming eruptive processes: Standing Rocks West, Hopi Buttes, Navajo Nation, USA. *Bull. Volcanol.* 75 (8), 739. doi:10.1007/s00445-013-0739-9

Loewen, M. W., and Bindeman, I. N. (2015). Oxygen isotope and trace element evidence for three-stage petrogenesis of the youngest episode (260–79 ka) of Yellowstone rhyolitic volcanism. *Contrib. to Mineral. Petrol.* 170, 1–25.

Lorenz, V. (2003). Maar-diatreme volcanoes, their formation, and their setting in hard-rock or soft-rock environments. *Geolines* 15, 63–74

Lorenz, V. (1973). On the formation of maars. *Bull. Volcanol.* 37 (2), 183–204. doi:10.1007/BF02597130

Lorenz, V. (1986). On the growth of maars and diatremes and its relevance to the formation of tuff rings. *Bull. Volcanol.* 48 (5), 265–274. doi:10.1007/BF01081755

Lorenz, V., Suhr, P., and Suhr, S. (2017). Phreatomagmatic maar-diatreme volcanoes and their incremental growth: A model. *Geol. Soc. Lond. Spec. Publ.* 446 (1), 29–59. doi:10.1144/SP446.4

Lustrino, M., and Wilson, M. (2007). The circum-Mediterranean anorogenic Cenozoic igneous province. *Earth-Science Rev.* 81 (1-2), 1–65. doi:10.1016/j.earscirev.2006.09.002

Martí, J., Planagumà, L., Geyer, A., Canal, E., and Pedrazzi, D. (2011). Complex interaction between Strombolian and phreatomagmatic eruptions in the Quaternary monogenetic volcanism of the Catalan Volcanic Zone (NE of Spain). *J. Volcanol. Geotherm. Res.* 201 (1–4), 178–193. doi:10.1016/j.jvolgeores.2010.12.009

McDonough, W. F., and Sun, S. -s. (1995). The composition of the Earth. *Chem. Geol.* 120 (3–4), 223–253. doi:10.1016/0009-2541(94)00140-4

Mouralis, D., Pastre, J.-F., Kuzucuoğlu, C., Türkecan, A., and Guillou, H. (2019). Tephrostratigraphy and chronology of the quaternary gölludağ and Acıgöl volcanic complexes (central Anatolia, Turkey). *Med. Geosc. Rev.* 1 (2), 179–202. doi:10.1007/s42990-019-00010-8

Mouralis, D., Pastre, J. F., Kuzucuoglu, C., Türkecan, A., Atici, Y., Slimak, L., et al. (2002). Les complexes volcaniques Rhyolithiques quaternaires d'Anatolie centrale (Göllü Dag et Acigöl, Turquie): Genèse, instabilité, contraintes environnementales. *Quaternaire* 13 (3), 219–228. doi:10.3406/quate.2002.1714

Németh, K., Goth, K., Martin, U., Csillag, G., and Suhr, P. (2008). Reconstructing paleoenvironment, eruption mechanism and paleomorphology of the Pliocene Pula maar, (Hungary). *J. Volcanol. Geotherm. Res.* 177 (2), 441–456. doi:10.1016/j.jvolgeores.2008.06.010

Newhall, C., Self, S., and Robock, A. (2018). Anticipating future Volcanic Explosivity Index (VEI) 7 eruptions and their chilling impacts. *Geosphere* 14 (2), 572–603. doi:10.1130/ges01513.1

Ort, M. H., Lefebvre, N. S., Neal, C. A., McConnell, V. S., and Wohletz, K. H. (2018). Linking the Ukinrek 1977 maar-eruption observations to the tephra deposits: New insights into maar depositional processes. *J. Volcanol. Geotherm. Res.* 360, 36–60. doi:10.1016/j.jvolgeores.2018.07.005

Özdemir, Y., Blundy, J., and Güleç, N. (2011). The importance of fractional crystallization and magma mixing in controlling chemical differentiation at Süphan stratovolcano, eastern Anatolia, Turkey. *Contrib. Mineral. Pet.* 162, 573–597. doi:10.1007/s00410-011-0613-8

Polacci, M., Pioli, L., and Rosi, M. (2003). The Plinian phase of the Campanian Ignimbrite eruption (Phlegrean Fields, Italy): Evidence from density measurements and textural characterization of pumice. *Bull. Volcanol.* 65 (6), 418–432. doi:10.1007/s00445-002-0268-4

Rabayrol, F., Hart, C. J., and Thorkelson, D. J. (2019). Temporal, spatial and geochemical evolution of late Cenozoic post-subduction magmatism in central and eastern Anatolia, Turkey. *Lithos* 336, 67–96. doi:10.1016/j.lithos.2019.03.022

Rasband, W. S. (2006). *ImageJ, v. 1.37*. Bethesda, MD, United States: U. S. National Institutes of Health. Available at: http://rsb.info.nih.gov/ij/

Reid, M. R., Schleiffarth, W. K., Cosca, M. A., Delph, J. R., Blichert-Toft, J., and Cooper, K. M. (2017). Shallow melting of MORB-like mantle under hot continental lithosphere, Central Anatolia. *Geochem. Geophys. Geosyst.* 18, 1866–1888. doi:10.1002/2016gc006772

Riggs, N. R., and Duffield, W. A. (2008). Record of complex scoria cone eruptive activity at Red Mountain, Arizona, USA, and implications for monogenetic mafic volcanoes. *J. Volcanol. Geotherm. Res.* 178 (4), 763–776. doi:10.1016/j.jvolgeores.2008.09.004

Roberts, N., Reed, J. M., Leng, M. J., Kuzucuoğlu, C., Fontugne, M., Bertaux, J., et al. (2001). The tempo of Holocene climatic change in the eastern Mediterranean region: New high-resolution crater-lake sediment data from central Turkey. *Holocene* 11 (6), 721–736. doi:10.1191/09596830195744

Ross, P.-S., Carrasco Núñez, G., and Hayman, P. (2017). Felsic maar-diatreme volcanoes: A review. *Bull. Volcanol.* 79 (2), 20. doi:10.1007/s00445-016-1097-1

Sato, H., and Taniguchi, H. (1997). Relationship between crater size and ejecta volume of recent magmatic and phreato-magmatic eruptions: Implications for energy partitioning. *Geophys. Res. Lett.* 24 (3), 205–208. doi:10.1029/96GL04004

Schmitt, A. K., Danišík, M., Evans, N. J., Siebel, W., Kiemele, E., Aydin, F., et al. (2011). Acigöl rhyolite field, Central Anatolia (part 1): High-resolution dating of eruption episodes and zircon growth rates. *Contrib. Mineral. Pet.* 162 (6), 1215–1231. doi:10.1007/s00410-011-0648-x

Sheridan, M. F., and Updike, R. G. (1975). Sugarloaf mountain tephra—a pleistocene rhyolitic deposit of base-surge origin in northern Arizona. *Geol. Soc. Am. Bull.* 86, 571–581. doi:10.1130/0016-7606(1975)86<571:smtapr>2.0.co;2

Siebel, W., Schmitt, A. K., Kiemele, E., Danišík, M., and Aydin, F. (2011). Acigöl rhyolite field, Central Anatolia (part II): Geochemical and isotopic (Sr–Nd–Pb, δ18O) constraints on volcanism involving two high-silica rhyolite suites. *Contrib. Mineral. Pet.* 162 (6), 1233–1247. doi:10.1007/s00410-011-0651-2

Simon, J. I., and Reid, M. R. (2005). The pace of rhyolite differentiation and storage in an "archetypical" silicic magma system, Long Valley, California. *Earth and Planetary Sci. Let.* 235, 123–140.

Søager, N., Portnyagin, M., Hoernle, K., Holm, P. M., Hauff, F., and Garbe-Schonberg, D. (2015). Olivine major and trace element compositions in southern Payenia basalts, Argentina: evidence for pyroxenite-peridotite melt mixing in a back-arc setting. *J. Petrol.* 56, 1495–1518.

Sohn, Y. K., and Chough, S. K. (1989). Depositional processes of the suwolbong tuff ring, cheju island (korea). *Sedimentology* 36 (5), 837–855. doi:10.1111/j.1365-3091.1989.tb01749.x

Streck, M. J., and Grunder, A. L. (2008). Phenocryst-poor rhyolites of bimodal, tholeiitic provinces: The rattlesnake tuff and implications for mush extraction models. *Bull. Volcanol.* 70, 385–401. doi:10.1007/s00445-007-0144-3

Sweeney, M. R., Grosso, Z. S., and Valentine, G. A. (2018). Topographic controls on a phreatomagmatic maar-diatreme eruption: Field and numerical results from the Holocene Dotsero volcano (Colorado, USA). *Bull. Volcanol.* 80 (11), 78. doi:10.1007/s00445-018-1253-x

Taddeucci, J., Sottili, G., Palladino, D. M., Ventura, G., and Scarlato, P. (2010). A note on maar eruption energetics: Current models and their application. *Bull. Volcanol.* 72 (1), 75–83. doi:10.1007/s00445-009-0298-2

Toprak, V., and Göncüoğlu, M. (1993). Tectonic control on the development of the neogene-quaternary central anatolian volcanic province, Turkey. *Geol. J.* 28, 357–369. doi:10.1002/gj.3350280314

Toprak, V. (1998). Vent distribution and its relation to regional tectonics, Cappadocian Volcanics, Turkey. *J. Volcanol. Geotherm. Res.* 85 (1–4), 55–67. doi:10.1016/S0377-0273(98)00049-3

Tuncer, A., Tunoğlu, C., Aydar, E., Yilmaz, İ. Ö., Gümüş, B. A., and Şen, E. (2019). Holocene paleoenvironmental evolution of the Acıgöl paleo maar lake (Nevşehir, Central Anatolia). *Med. Geosc. Rev.* 1 (2), 255–269. doi:10.1007/s42990-019-00009-1

Türkecan, A., Kuzucuoğlu, C., Mouralis, D., Pastre, J., Atıcı, Y., Guillou, H., et al. (2004). *Upper pleistocene volcanism and palaeogeography in cappadocia, Turkey*. Ankara: Tech. rep., TUBITAK Project No.101Y109. MTA Report No.10652.

Uieda, L., Tian, D., Leong, W., Toney, L., Schlitzer, W., Grund, M., et al. (2021). *PyGMT: A Python interface for the generic mapping tools.*

Ulusoy, I., Labazuy, P., Aydar, E., Atak, O., Yürür, T., Artuner, H., et al. (2009). *Multisource geophysical investigation of the Acigöl caldera structure (central Turkey): Preliminary results*. Vienna, Austria: EGU General Assembly, 7746.

Ureta, G., Németh, K., Aguilera, F., Zimmer, M., and Menzies, A. (2021). A window on mantle-derived magmas within the Central Andes: Eruption style transitions at Cerro Overo maar and La Albóndiga lava dome, northern Chile. *Bull. Volcanol.* 83 (4), 19. doi:10.1007/s00445-021-01446-3

Uslular, G., and Gençalioğlu-Kuşcu, G. (2019). Mantle source heterogeneity in monogenetic basaltic systems: A case study of Eğrikuyu monogenetic field (central Anatolia, Turkey). *Geosphere* 15, 295–323. doi:10.1130/ges01682.1

Uslular, G., Le Corvec, N., Mazzarini, F., Legrand, D., and Gençalioğlu-Kuşcu, G. (2021). Morphological and multivariate statistical analysis of Quaternary monogenetic vents in the Central Anatolian Volcanic Province (Turkey): Implications for the volcano-tectonic evolution. *J. Volcanol. Geotherm. Res.* 416, 107280. doi:10.1016/j.jvolgeores.2021.107280

Valentine, G. A., Krier, D., Perry, F. V., and Heiken, G. (2005). Scoria cone construction mechanisms, Lathrop Wells volcano, southern Nevada, USA. *Geology* 33 (8), 629–632. doi:10.1130/G21459AR.1

Valentine, G. A., White, J. D. L., Ross, P.-S., Graettinger, A. H., and Sonder, I. (2017). Updates to concepts on phreatomagmatic maar-diatremes and their pyroclastic deposits. *Front. Earth Sci. (Lausanne).* 5, 68. doi:10.3389/feart.2017.00068

van Otterloo, J., Cas, R. A. F., and Sheard, M. J. (2013). Eruption processes and deposit characteristics at the monogenetic Mt. Gambier Volcanic Complex, SE Australia: Implications for alternating magmatic and phreatomagmatic activity. *Bull. Volcanol.* 75 (8), 737. doi:10.1007/s00445-013-0737-y

White, J. D. L., and Houghton, B. F. (2006). Primary volcaniclastic rocks. *Geol.* 34 (8), 677. doi:10.1130/G22346.1

White, J. D. L., and Ross, P.-S. (2011). Maar-diatreme volcanoes: A review. *J. Volcanol. Geotherm. Res.* 201 (1–4), 1–29. doi:10.1016/j.jvolgeores.2011.01.010

Yalınız, K. M., Aydin, N. S., Göncüoğlu, M. C., and Parlak, O. (1999). Terlemez quartz monzonite of central Anatolia (Aksaray–Sarıkaraman): Age, petrogenesis and geotectonic implications for ophiolite emplacement. *Geol. J.* 34, 233–242. doi:10.1002/(sici)1099-1034(199907/09)34:3<233:aid-gj824>3.0.co;2-5

Yıldırım, T., and Özgür, R. (1981). Acıgöl kalderası. *Jeomorfol. Derg.* 10, 59–70.

Zimanowski, B., Buttner, R., and Lorenz, V. (1997). Premixing of magma and water in MFCI experiments. *Bull. Volcanol.* 58, 491–495. doi:10.1007/s004450050157

Zimmer, B. W., Riggs, N. R., and Carrasco-Núñez, G. (2010). Evolution of tuff ring-dome complex: The case study of Cerro Pinto, eastern Trans-Mexican Volcanic Belt. *Bull. Volcanol.* 72 (10), 1223–1240. doi:10.1007/s00445-010-0391-6